A CRETACEOUS PHONOLITE DYKE FROM THE TOMAHAWK RIVER, NORTHEAST TASMANIA

by J. L. Everard, F. L. Sutherland and H. Zwingmann

(with 11 tables, 13 text-figures and six plates)

EVERARD, J. L., SUTHERLAND, F. L. & ZWINGMANN, H., 2004 (29.x): A Cretaceous phonolite dyke from the Tomahawk River, northeastTasmania. *Papers and Proceedings ofthe Royal Society ofTasmania* 138: 11-33.
https://doi.org/10.26749/rstpp.138.11 ISSN 0080-4703.Tasmanian Geological Survey, Mineral ResourcesTasmania, PO Box 56, Rosny Park, Tasmania 7018, Australia (JLE*); Geodiversity Research Centre, Australian Museum, 6 College Street, Sydney, New South Wales 2010, Australia (FLS); CSIRO Division of Petroleum Resources and Centre of Excellence in Mass Spectrometry, School of Applied Geology, Curtin University, Western Australia 6102, Australia (HZ).
*Author for correspondence.

Field mapping and ground magnetics indicate that a phonolite dyke, which intrudes Devonian granite in the upper Tomahawk River area, Tasmania, is 3.2 km long and shallowly west-dipping wirh a true thickness of 10–15 m. The rock contains microphenocrysts of anorthoclase, sparse fayalitic olivine and low-Ti magnetite, and rare biotite in a groundmass of aligned alkali feldspar laths, with interstitial clinopyroxene (hedenbergite to aegirine), amphibole (either hastingsite or arfvedsonite), sodalite, nepheline, analcime and accessory apatite. It is peralkaline and exceptionally strongly evolved, even for phonolites, with very low TiO_2, MgO and CaO, and high Na_2O and incompatible elements. However, relatively high Sr and Ba and the absence of a negative Eu anomaly suggest little feldspar fractionation in its petrogenesis. Its Late Cretaceous age (K/Ar 80.4 ± 1.6 Ma, $^{40}Ar/^{39}Ar$ plateau 75.8 ± 0.3 Ma, $^{40}Ar/^{39}Ar$ total fusion 76 ± 3.1 Ma) and geochemistry are unique for Tasmania and it represents a newly recognised, although very minor, igneous episode. It may be related to a change in dynamic regime following continental rifting, the opening of rhe Tasman Sea and the subsidence of Bass Basin.

Key Words: phonolite, peralkaline rocks, pyroxenes, amphiboles, arfvedsonite, K/Ar dating, $^{40}Ar/^{39}Ar$ dating, Cretaceous, Tasmania.

INTRODUCTION

Phonolites are felsic, volcanic or hypabyssal igneous rocks which, despite their relatively high SiO_2 content, are undersaturated in silica because of their very high alkali content ($Na_2O + K_2O$). Their most voluminous development is in and around the East African Rift Valley (e.g., Lippard 1973, Price *et al.* 1985). Elsewhere they are relatively uncommon and usually subordinate to associated mafic rocks. There are well-documented Cainozoic examples in other continental settings, usually also related to rifting, such as the Rhine Graben (e.g., Wörner & Schmincke 1984a, b), the Massif Central of France (Wilson *et al.* 1995) and the McMurdo Volcanic Province, which includes Mt Erebus, Antarctica (Kyle 1981, Kyle *et al.* 1992). Recently studied intra-plate oceanic examples occur on Tristan da Cunha (Le Roex *et al.* 1990), Tenerife (Ablay *et al.* 1998), Fernando de Noronha and Trinidade (Weaver 1990), Rarotonga (Thompson *et al.* 2001), Kaula, Hawaii (Garcia *et al.* 1986) and McDonald Island, Southern Ocean (Quilty & Wheller 2000). These are associated with ocean island basalts (OIB) and, together with the McMurdo Volcanic Province, appear to be related to upwelling mantle plumes ("hotspots"). Phonolites are rare in subduction-related or orogenic environments (e.g., Keller 1983, Sorensen 1974).

There are limited occurrences of phonolite, of Jurassic to Late Cainozoic age, in eastern Australia (Ewart *et al.* 1985, Knutson 1989, Sutherland *et al.* 1996). They have not been recorded previously in Tasmania, although feldspathoidal syenite, their approximate plutonic equivalent, is a subordinate component of the Cretaceous Cygnet alkaline complex (Edwards 1947, Ford 1983, Taheri & Bottrill 1999). A plug of Cainozoic basalt at Droughty Point near Hobart contains small (≤ 40 mm) coarse-grained late-stage segregations, some of which approach mafic phonolite in composition (Sutherland 1976).

PREVIOUS WORK

Baillie (1972) reported outcrops of dark green "lamprophyre" at three localities (EQ641638, EQ638646, EQ636652 (grid references refer to 1:25,000 Monarch (5646) and 1:100,000 Cape Portland (8416) topographic sheets; datum is AGD66) in the valley of the Tomahawk River, about 9–12 km south of Tomahawk township. They were thought to indicate a NNW-trending post-granitic dyke of unknown length but not more than 6 m wide. The rock was described as consisting of phenocrysts (25%) of oriented albite (80%), olivine (15%), lamprobolite amphibole (4%) and pyrite (1%) in an extremely fine-grained panidiomorphic granular groundmass containing a faintly green mineral, possibly actinolite.

On the Boobyalla 1:50,000 geological map (Baillie *et al.* 1978), the dyke is labelled "Ca?", a unit also used for Cretaceous appinitic rocks near Cape Portland (Jennings & Sutherland 1969). The dyke is shown as extending for about 1.5 km, partly concealed by Quaternary alluvium, with another small exposure 1.5 km further north, slightly offset to the east (EQ635664).

The local country rock is granite, comprising the Poimena and Little Mt Horror plutons of the Blue Tier Batholith (figs 1, 2; Groves 1977). Probably the most reliable published radiometric date from the Poimena pluton is a Rb-Sr mineral isochron of 379 ± 3 Ma (Middle Devonian) (McKenzie *et al.* 1988), although an unpublished SHRIMP U-Pb zircon age is about 5 Myr older (L. P. Black pers. comm.). On the

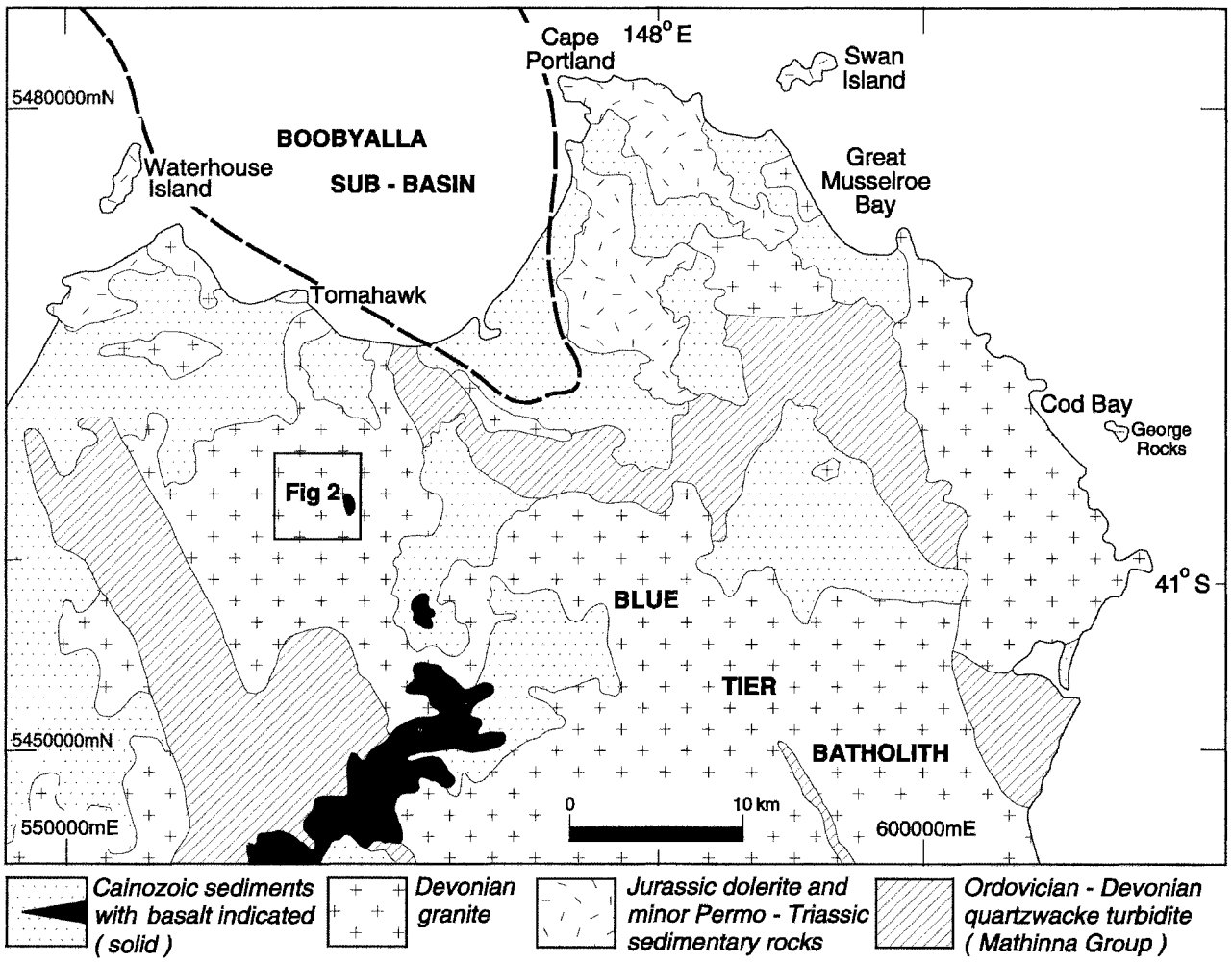

FIG. 1 — Simplified geology of part of northeast Tasmania showing location of Tomahawk River dyke and localities mentioned in text.

basis of intrusive relationships, the Little Mt Horror pluton is thought to be slightly younger than the Poimena pluton (Baillie 1972, McClenaghan *et al.* 1982).

FIELD RELATIONS AND GEOPHYSICS

The phonolite is a tough, dark bluish- to greenish-grey, fine-grained, massive aphanitic rock with locally well-developed platy jointing. Eight samples collected for petrological examination (table 1) are registered and stored at Mineral Resources Tasmania, Mornington.

The dyke can be traced along strike for about 3.2 km and has a slightly arcuate NNW to northerly trend (fig. 2). Its most southerly exposure is on the west bank of the Tomahawk River (EQ64106364), beyond which only granite was encountered. To the north, the dyke largely forms float on a series of low rocky knolls in rough pasture and light forest. In small cliffs just west of the river (EQ63376572), a steep western contact with fine-grained granite is exposed; here the dyke is about 20 m wide. About 400 m further north (near 63406620) a fault may offset the dyke dextrally by about 100 m, but outcrop is poor and a change in strike is possible. The dyke re-appears immediately west of a small gorge in the river (EQ63516633), and scattered float and rubbly outcrop continue for a further 400 m to EQ63476672.

The phonolite has a moderately high mean magnetic susceptibility of about 5.35 x 10^{-3} SI units (table 1) but it is not apparent on images of the area derived from regional aeromagnetic data (BMR, 1985). However, this survey had a 1.5 km line spacing and a 150–1000 m terrain clearance, probably inadequate to resolve any associated anomaly.

In order to constrain the dimensions and orientation of the body, six ground magnetometer traverses were measured across its southern segment, roughly perpendicular to strike (fig. 2). Survey details, data and interpretation are described in detail by Everard (2004).

The two northern profiles (A–A' and B–B') each contain an asymmetric anomaly peaking at about 60 nT above the local regional field, accompanied by a smaller negative anomaly to the east. They are easily modelled by a dipping dyke with a true thickness of 10–15 m, dipping west at 18–31° and extending very close to the surface. Profile D–D' is similar but was not modelled due to distortion of the field by several wire fences.

Profile C-C' defines a much broader and more subdued (15 nT) anomaly, consistent with a dyke dipping west at about 30°. It may have a maximum true thickness of about 13 m at a depth of 40 m, tapering out both downward and within about 2 m of the surface.

Profile E–E' is complex with several distinct peaks of up to about 50 nT spread out over an east-west distance of about 120 m, accompanied by a distinct negative anomaly to the

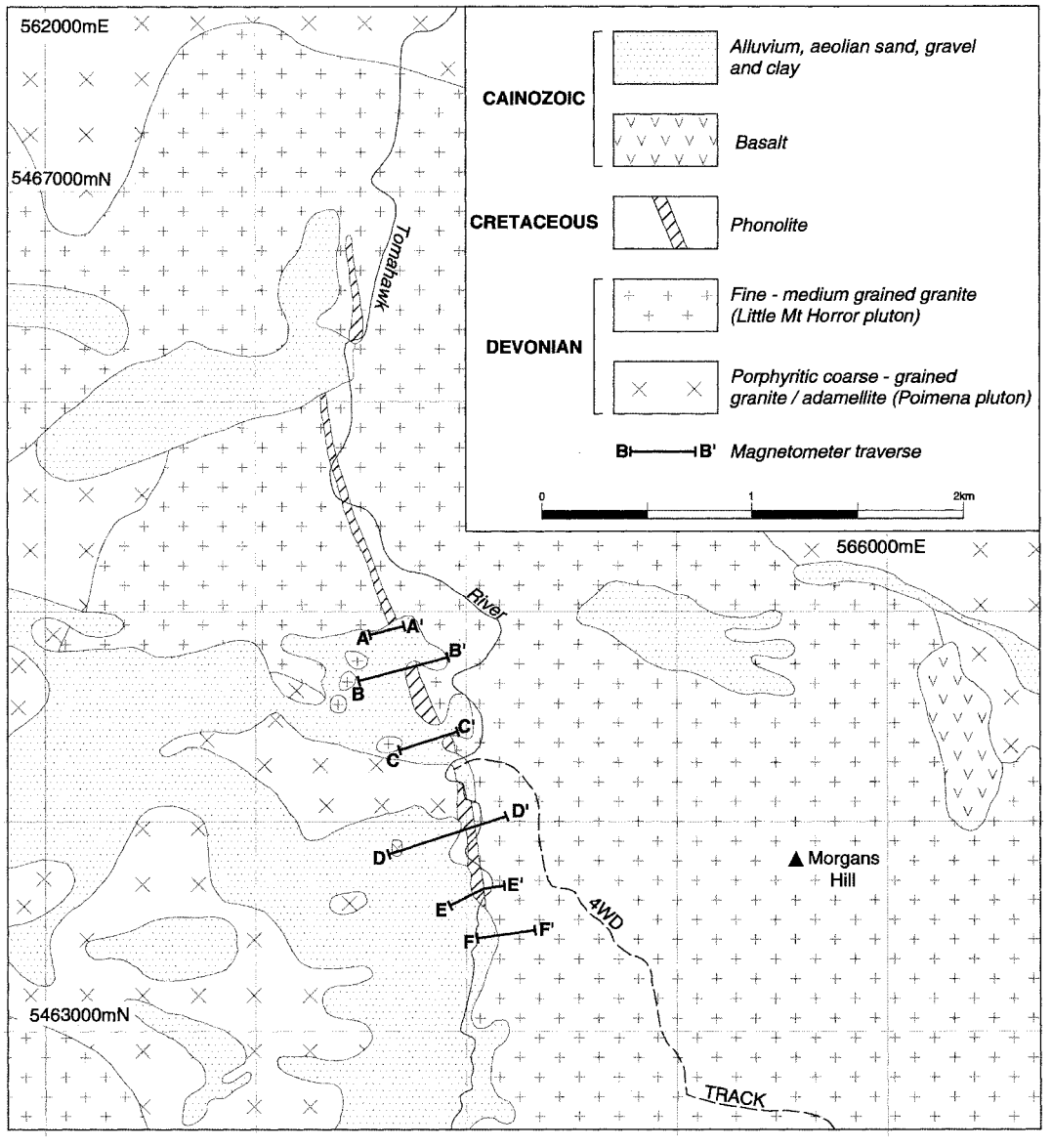

FIG. 2 — Detailed geology of upper Tomahawk River area (modified after Baillie et al. *1978) showing phonolite dyke and location of magnetometer traverses.*

TABLE 1
Sample locations and physical properties

Field no.	Reg. no.	metres E	metres N	Magnetic susceptibility (x10^{-3} SI)				Density
		datum:AGD66		N	mean	min	max	t/m^3
PHN[a]	C108641	563640	5465010					
PHS[a,b]	C108642	563770	5464660					
CPJ32[a,b]	R006569	564100	5463640	10	5.64	4.85	6.53	2.642
CPJ33[a]	R006570	564110	5463690					
CPJ38	R004373	563770	5464630					
CPJ39	R004374	563510	5465380					
CPJ40	R004375	563510	5466440	10	6.19	5.22	7.44	2.628
CPJ41[a]	R004376	563350	5465990	20	4.78	2.45	6.31	2.605

[a] mineral (electron microprobe) analyses (tables 4–10)

[b] whole rock analyses (table 11)

west. Modelling suggests that here the main dyke may be split into five sub-parallel splays, none more than about 10 m thick, each dipping west at about 30°. These may taper and pinch out southward, as profile F–F', about 200 m south of the southernmost phonolite outcrop, contains two small overlapping positive anomalies of about 12 nT and 8 nT, consistent with two thin (3–4 m) west-dipping dykes concealed by about 10 m of overburden.

GEOCHRONOLOGY

K-Ar Analysis

The selected sample CPJ32, with least alteration of K-bearing phases, was ground to 750 μm. K contents were determined by atomic absorption (Varian AA20), following procedures after Heinrichs & Herrmann (1990). The pooled error of duplicate K determinations and standards is better than 2%. K-Ar isotope determinations followed Bonhomme *et al.* (1975) and spiked isotopes were measured in a high sensitivity VG 3600 noble-gas mass spectrometer. The ^{38}Ar spike was calibrated against biotite GA1550 (95.5 Ma, McDougall & Roksandic 1974) together with measurements of standards (LP-6, HD-B1, GLO and GA 1550) and mass discrimination factors (airshots). Errors for Ar analysis were <1% and $^{40}Ar/^{36}Ar$ values for airshots were 293.39 ± 0.29 (2σ). The result with 2σ error (table 2) used ^{40}K abundances and decay constants recommended by Steiger & Jäger (1977).

^{40}Ar–^{39}Ar analysis

A detailed account of the ^{40}Ar-^{39}Ar dating technique (McDougall & Harrison 1999) underpins the dating presented here. A concentrate of separated feldspar from the rock was cleaned before wrapping in aluminium foil for loading into an aluminium package, along with biotite standard HD-B1 (24.21 ± 0.32 Ma, Hess & Lippolt 1994) to monitor the neutron flux gradient. The package was Cd-shielded and fast neutron irradiated in the McMaster University Nuclear Reactor, Hamilton, Canada, for 28.4 hours.

For infra-red laser step-heating, the mineral separate was loaded onto an aluminium palette and baked within an ultra-high vacuum laser sample chamber to 120°C overnight to remove absorbed atmospheric argon. A 110 W Spectron Laser systems continuous wave Nd-Y-Al-garnet (= λ1064 nm) laser was used to laser step treat the sample.

Gas cleanup and mass spectrometry removed active gases using Zr-Al getter pumps and the remaining noble gases were equilibrated into a Mass Analyser Product 215-50 static mass spectrometer with a Balzers multiplier detector. The Ar sensitivity of the ms multiplier detector was 2.71 x 10^{-10} cm^3/Volt. A Lab View program was used to measure isotope peak masses from 35–41 (10 times) in sequence lasting ~15 minutes, via a peak hopping routine. Blank analyses were run before and after.

Age calculation involved extrapolating peak intensities back to the inlet time and correcting for extraction line blanks, ms backgrounds, ms discrimination ($^{40}Ar/^{36}Ar$ ratio of 281.0) and reactor interferences. The Ca and K correction factors in the data reduction were $^{39}Ar/^{37}Ar_{Ca}$ = 0.00065, $^{36}Ar/^{37}Ar_{Ca}$ = 0.000255 and $^{40}Ar/^{36}Ar_{K}$ = 0.0015). Errors quoted are 1σ and Ar-Ar ages were calculated using decay constants of Steiger & Jäger (1977). Weighted mean ages were calculated (2σ errors) using the Ludwig (2001) Isoplot program (fig. 3).

TABLE 2
K-Ar analysis

Sample	%K (duplicate)	$^{40}Ar^a$ ($x10^{-3}$ mol/g)	$^{40}Ar/^{40}Ar_{total}$	Age (Ma)	Error (±2δ)
CPJ32	3.31	4.720	0.927	80.40	1.60

[a] Denotes radiogenic argon.
Constants: ^{40}K = 0.01167 atom 96; λβ = 4.962, λε = 0.581 x $10^{-10}y^{-1}$

Results

The K-Ar results (table 2) give an age of 80.40 ± 1.60 Ma. The Ar-Ar analysis (table 3, fig. 3) gives a weighted mean age of 75.77 ± 0.32 Ma from steps 4–5 (lowest-Ca steps and highest ^{40}Ar *yields) and a total fusion age of 76 ± 3.1 Ma. There was evidence of mixing with a Ca-rich phase in the feldspar separate. The total fusion Ar-Ar and K-Ar age are within error and with the weighted mean Ar-Ar age confirm a Late Cretaceous age for the phonolite crystallisation, with age limits between 75 and 81 Ma. On recent time-scales (e.g., Young & Laurie 1996) this is within the Campanian (73–83 Ma).

PETROGRAPHY

In thin section (pls 1–6), the samples are similar. Most are slightly porphyritic (pl. 1) to seriate (pl. 2), with microphenocrysts of anorthoclase (≤ 1.5 mm but commonly 500 μm–1 mm long) grading down in grain size to a usually pilotaxitic groundmass. Sparse to rare, usually corroded microphenocrysts include fayalite (≤ 0.1–1.0% by volume), magnetite (c. 0.3–1%) and rare biotite. These minerals are rare in the groundmass, probably due to a reaction relationship with it (pls 3, 4, 5).

The groundmass (pls 5, 6) consists of flow-aligned laths (commonly 50–100 μm long) of alkali feldspar (mainly anorthoclase), small platelets and prisms of clinopyroxene (hedenbergite to aegirine) and amphibole (hastingsite and/or arfvedsonite), together with interstitial sanidine, feldpathoids, zeolites, minor pale brown, slightly turbid glass, accessory apatite, and sometimes traces of biotite.

Electron microprobe analyses (see below) and X-ray diffraction of powdered samples indicate that the feldspathoids are nepheline and sodalite. The main zeolite is analcime, with substantial natrolite in CPJ39. Their identification is supported by the disappearance of their diffraction peaks after treatment of the powders with dilute HCl, which dissolves these minerals (R. N. Woolley, pers. comm.). Reconnaissance scanning electron microscope work (R. S. Bottrill) suggests the presence of small amounts of a Na-Ca silicate, possibly pectolite, as minute grains in one sample (PHS). The presence of pyrite, reported in the dyke by Baillie (1972), has not been substantiated.

There are small variations between samples in the abundance of feldspar microphenocrysts, groundmass

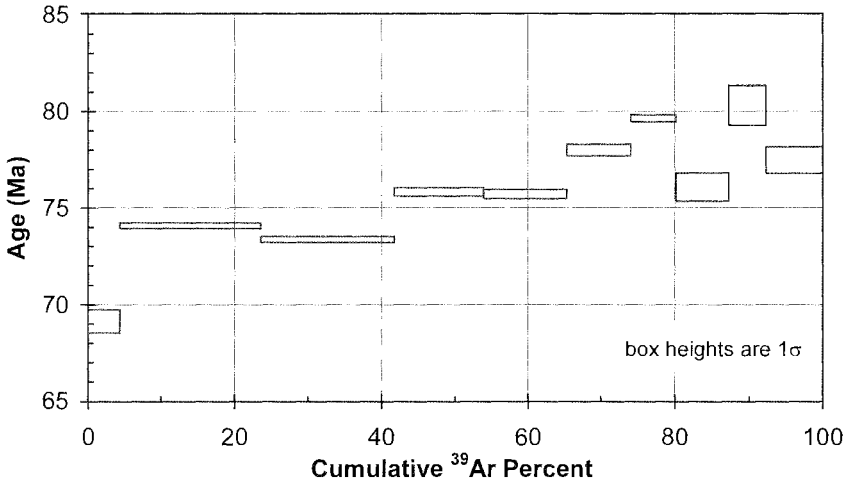

FIG. 3 — Step heating age spectrum (apparent age versus cumulative ^{39}Ar released) for ^{40}Ar/^{39}Ar analysis, Tomahawk phonolite sample CPJ32.

TABLE 3
^{40}Ar-^{39}Ar analysis, Tomahawk River phonolite; sample 412 (K-feldspar from sample CPJ32)

Step	Age (Ma)	^{40}Ar*/^{39}Ar	^{40}Ar/^{39}Ar	^{38}Ar/^{39}Ar	^{37}Ar/^{39}Ar	^{36}Ar/^{39}Ar	^{39}Ar (10^{-12}cm^3)	40Ar* (%)
1	69.13±0.69	5.90±0.05	7.49±0.01	0.01287±0.00035	0.06238±0.00417	0.00539±0.00017	77.74±0.06	78.7
2	74.08±0.39	6.33±0.01	7.08±0.01	0.01299±0.00011	0.04164±0.00095	0.00539±0.00004	342.45±0.22	89.3
3	73.36±0.39	6.26±0.01	6.79±0.01	0.01532±0.00008	0.03488±0.00100	0.00178±0.00004	324.82±0.24	92.2
4	75.83±0.43	6.48±0.02	6.97±0.01	0.01363±0.00012	0.02630±0.00067	0.00167±0.00006	218.22±0.16	92.9
5	75.72±0.44	6.47±0.02	6.88±0.01	0.01335±0.00013	0.02598±0.00143	0.00139±0.00007	204.05±0.16	94.0
6	78.00±0.48	6.67±0.03	7.26±0.01	0.01390±0.00017	0.02833±0.00186	0.00199±0.00009	156.00±0.09	91.9
7	79.64±0.43	6.81±0.02	7.33±0.02	0.01392±0.00013	0.02709±0.00006	0.00174±0.00000	108.85±0.24	93.0
8	76.08±0.82	6.50±0.06	7.38±0.01	0.01415±0.00024	0.05120±0.00230	0.00298±0.00021	126.75±0.08	88.1
9	80.31±1.09	6.87±0.09	7.49±0.01	0.01360±0.00030	0.04923±0.00972	0.00210±0.00030	89.96±0.08	91.7
10	77.47±0.78	6.62±0.06	7.44±0.02	0.01256±0.00020	0.03444±0.00672	0.00276±0.00020	137.22±0.27	89.0

Total fusion age = 75.96 ± 3.10 Ma
Irradiation standard used = HD-B1 biotite (24.21 ± 0.32 Ma)
J value = 0.006510 ± 0.000032
1σ errors
Weighted mean age (steps 4–5) = 75.77 ± 0.60 Ma (2σ)

grain-size, development of flow lamination and degree of alteration (especially of feldspar). In particular, CPJ38 and CPJ39 (pl. 3) are aphyric and relatively coarse-grained with randomly oriented feldspars (typically 400–600 μm x 50–100 μm), and may be slower-cooled rocks from near the centre of the dyke.

MINERALOGY AND MINERAL CHEMISTRY

Minerals from five polished thin sections were analysed using the Cameca SX-50 electron microprobe at the University of Tasmania. Representative analyses and calculated cation formulae are given in tables 4–10 and full data by Everard (2004).

The amphibole arfvedsonite is a new mineral species for Tasmania, although there is a very old and spurious record from Swan Island (Anon 1970).

Olivine (fayalite)

Pale yellow fayalite occurs sometimes as equant to oblong euhedral microphenocrysts (≤1 mm) (pls 1, 2) with slightly corroded, ragged margins, but commonly as deeply-embayed subhedra (typically 400–500 μm) (pls 2, 4) or anhedral granules (c. 100 μm) (pl. 3). Some of the larger microphenocrysts contain inclusions of apatite, as rod-like laths (up to 100 x 15 μm) and hexagonal sections (up to 120 μm across). In some samples, fayalite is altered to orange to amber-coloured fibrous alteration products (CPJ33) or dark red-brown "iddingsite" (PHS).

Analyses (table 4, fig. 4) are near-stoichiometric with significant MnO (≤4.25%) and MgO (≤3.83%) but a narrow compositional range ($Fa_{86.3\text{-}89.0}$ $Fo_{4.4\text{-}9.2}$ $Jo_{3.6\text{-}6.0}$). The CaO contents (0.28–0.59%) are those of low pressure, volcanic olivine (≥0.10%) rather than plutonic olivine (≤0.10%)(Simkin & Smith 1970).

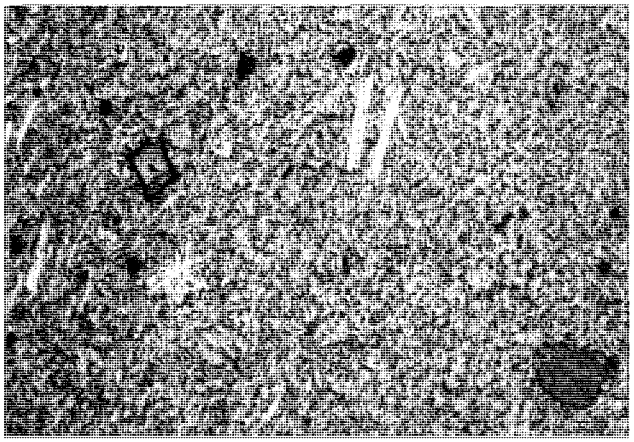

PLATE 1

Photomicrograph of phonolite (PHS), showing porphyritic texture with microphenocrysts of fayalite (left), anorthoclase (e.g., upper centre) and corroded biotite (lower right) in a fine-grained pilotaxitic groundmass (plane polarised light, field of view 4.5 x 3.4 mm).

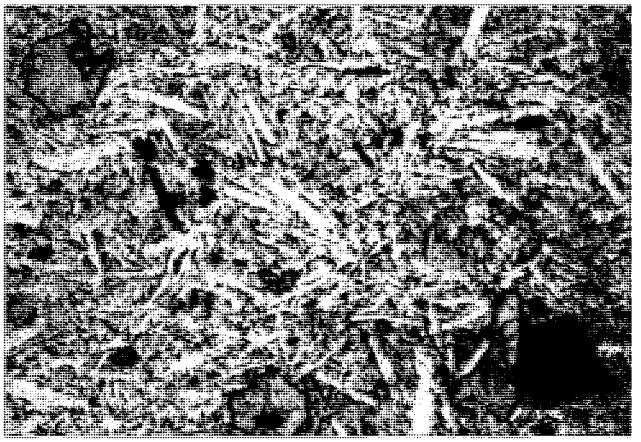

PLATE 2

Photomicrograph of phonolite (CPJ32), showing porphyritic to seriate texture with microphenocrysts of fayalite (upper left, centre bottom, lower right), magnetite (lower right) and anorthoclase grading to the groundmass (plane polarised light, field of view 4.5 x 3.4 mm).

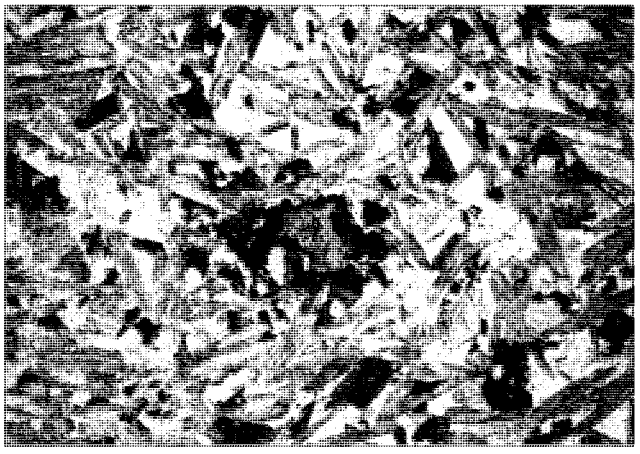

PLATE 3

Photomicrograph of phonolite (CPJ39), showing aphyric, relatively coarse-grained texture of mainly pyroxene and amphibole (dark), turbid alkali feldspar (grey) and interstitial feldspathoids and zeolites (clear). A central corroded fayalite grain has a narrow reaction rim of biotite and magnetite (plane polarised light, field of view 4.5 x 3.4 mm).

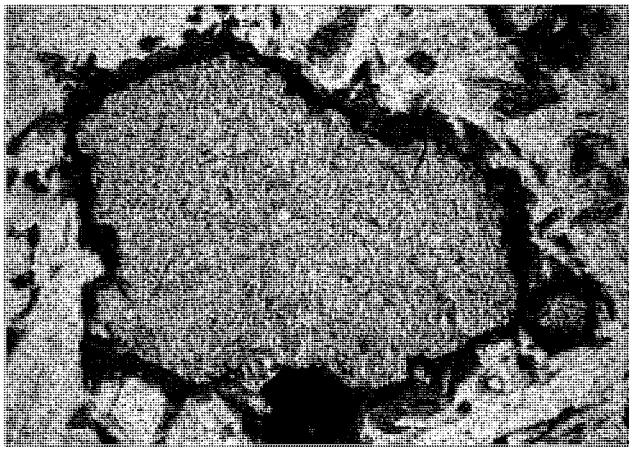

PLATE 4

Photomicrograph of phonolite (CPJ32) showing a corroded fayalite microphenocryst and abutting small magnetite microphenocryst (bottom), with narrow reaction rims of biotite (plane polarised light, field of view 730 x 550 μm).

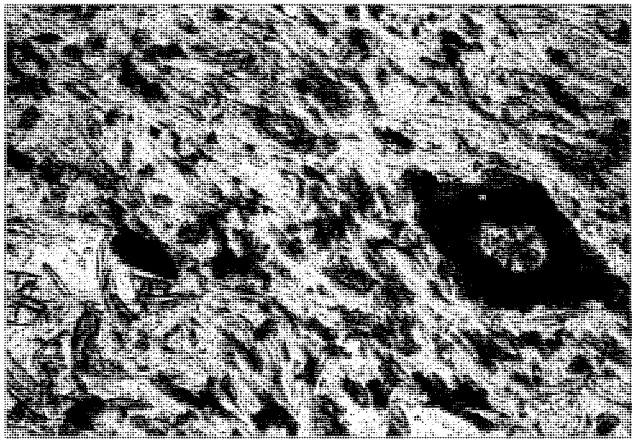

PLATE 5

Photomicrograph of phonolite (PHS) groundmass, showing aligned alkali feldspar laths with prisms of aegirine (grey) and arfvedsonite (dark grey, e.g., centre left). A fayalite granule (centre right) has a reaction rim of arfvedsonite (plane polarised light, field of view 730 x 550 μm).

PLATE 6

Photomicrograph of phonolite (PHS) groundmass, showing prisms and sections of arfvedsonite (dark, e.g., left) and aegirine (e.g., centre right) with feldspars, feldspathoids, zeolite and acicular apatite (e.g., upper left)(plane polarised light, field of view 280 x 210 μm).

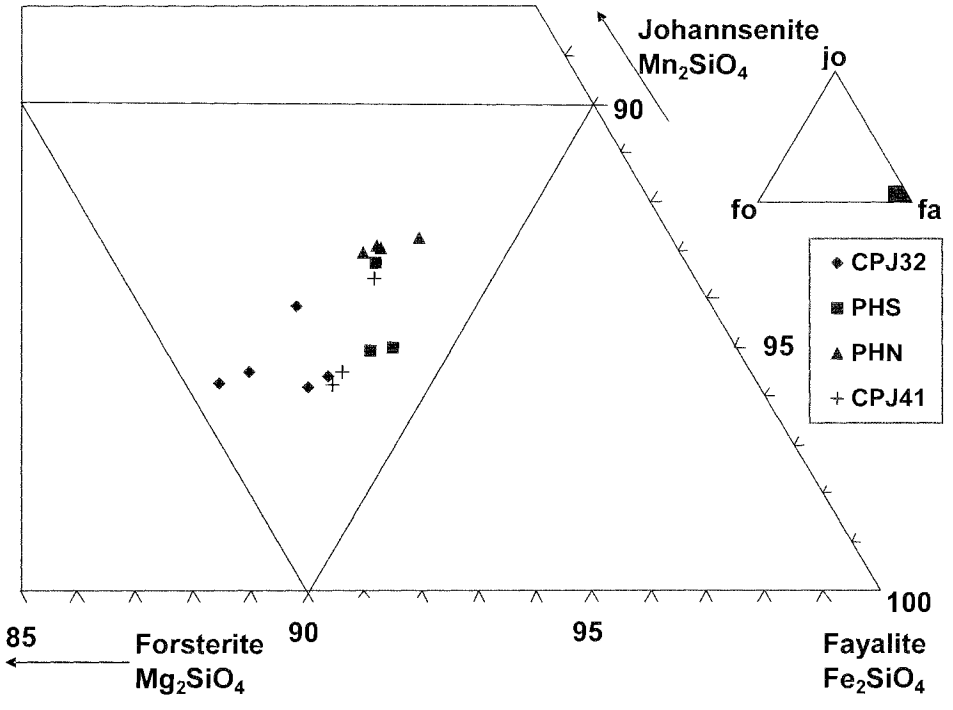

FIG. 4—Electron microprobe analyses of olivine (fayalite) phenocrysts, plotted in the plane Mg_2SiO_4 (forsterite)–Fe_2SiO_4 (fayalite)–Mn_2SiO_4 (johannsenite); small amounts of Ca_2SiO_4 component are included with Mn_2SiO_4.

TABLE 4
Representative mineral analyses: olivine (fayalite) phenocrysts

Sample	CPJ32	PHS	PHN
Analysis	R1/1	R7/4	R5/1
SiO_2	30.40	29.87	29.52
TiO_2	–	0.03	0.01
Cr_2O_3	0.02	0.01	–
FeO	63.34	64.16	63.20
MnO	2.75	3.21	4.18
NiO	0.07	–	–
MgO	3.83	2.42	1.78
CaO	0.30	0.31	0.76
Total	100.72	100.02	99.45
Cations calculated on the basis of (O) = 4			
Si	0.995	0.995	0.993
Ti	–	0.001	–
Cr	0.001	–	–
Fe^{II}	1.734	1.787	1.778
Mn	0.076	0.091	0.119
Ni	0.002	–	–
Mg	0.187	0.120	0.089
Ca	0.011	0.011	0.028
Total	3.005	3.004	3.007
Mg#	9.73	6.31	4.77

Magnetite

Opaque microphenocrysts (pls 2, 4) are equant, angular, polygonal (squarish to pseudohexagonal) to irregular or skeletal grains, exceptionally up to 1.5 x 1 mm, but commonly 150–400 μm across. They are identified in reflected light as magnetite, and can be drawn off the powdered samples by a magnet. Some of the larger microphenocrysts contain small (≤50 μm) inclusions of biotite and euhedral apatite. Usually, opaque phases are absent in the groundmass, except for rare small (c. 50 μm) partly oxidised magnetite grains in PHN.

Analyses (table 5) match low-Ti magnetite (TiO_2 ≤6.24%) in which Al_2O_3 (≤3.29%) and MnO (≤0.60%) are minor components. These values correspond to ≤18.0 mole % ulvospinel and ≤4.6 mole % hercynite in solid solution.

Biotite

Biotite is an uncommon mineral in the phonolite, but has three distinct parageneses. All are iron-rich biotites (table 6) with low fluorine (≤0.15%) and chlorine (≤0.13%), with compositions between annite and siderophyllite (fig. 5a).

Biotite microphenocrysts (α, β very dark sepia-brown, γ pale honey-yellow) are rare (< 0.1 %), rounded and corroded, apparently partly resorbed anhedra, up to 700 x 380 μm across (pl. 1). They are iron-rich (Mg# 8.4–18.7) with high tetrahedrally coordinated Al^{iv} (2.44–2.59 cations per formula unit), balanced by substitution of small amounts of Ti (TiO_2 ≤ 1.54%) and Al^{vi} into the octahedral sites. MnO (≤0.54%) and CaO (≤0.28%) are low.

Rare small ragged biotite is present in the groundmass of some samples. Analyses (from PHN) have similar Mg# (9.0–13.4) and Al^{iv} (2.35–2.50 cations/formula unit) to the microphenocrysts but lower TiO_2 (0.53–0.77%) (fig. 5b) and slightly higher MnO (0.60–1.62%) and CaO (≤0.57%).

TABLE 5
Representative mineral analyses: magnetite

Sample	CPJ32	PHS	CPJ33	CPJ41
Analysis	R1/3	R14a/1	m4	R11/2
SiO_2	0.33	0.30	0.33	0.30
TiO_2	4.72	2.24	6.24	1.81
ZrO_2	–	0.08	–	0.06
Al_2O_3	3.17	1.29	3.00	1.87
Cr_2O_3	0.02	0.03	–	0.01
FeO_t	84.98	89.20	82.43	90.04
MnO	0.44	0.59	0.66	0.42
ZnO	0.02	–	0.25	–
MgO	0.19	0.05	0.15	0.03
CaO	0.01	–	0.02	0.01
Total	93.89	93.78	93.09	94.54
cations calculated on the basis of Z = 3, (O) = 4				
Ti	0.135	0.064	0.180	0.052
Zr	–	0.002	–	0.001
Al	0.142	0.058	0.136	0.083
Cr	0.001	0.001	–	–
Fe^{III}	1.588	1.809	1.504	1.811
Fe^{II}	1.109	1.044	1.142	1.037
Mn	0.014	0.019	0.022	0.013
Zn	0.001	–	0.007	–
Mg	0.011	0.003	0.009	0.002
Ca	0.001	–	0.001	–
end-members (mole %)				
$Fe^{II}_2TiO_4$	13.47	6.59	18.00	5.26
$Fe^{II}Al_2O_4$	4.47	0.68	2.98	2.63
$Fe^{II}Fe^{III}_2O_4$	79.41	90.46	75.21	90.56
other	2.65	2.27	3.81	1.55

Fayalite and magnetite microphenocrysts commonly exhibit a narrow (5–10 μm) discontinuous reaction rim of granular biotite (pleochroic from deep orange-brown to almost opaque), surrounded by a concentration of green amphibole and pyroxene which passes into the groundmass (pls 3, 4). The biotite rims are low in TiO_2 (≤0.9%), relatively high in MnO (0.9–1.69%) and similar to groundmass biotite. A biotite inclusion within a magnetite phenocryst in CPJ33 has exceptionally low Mg# (0.70) and relatively high TiO_2 (1.81%).

Resorption of the biotite microphenocrysts suggests disequilibrium with the melt at emplacement. However, they are probably not xenocrysts derived from the granitic country rock, as the phonolite lacks other granite-derived xenocrysts such as quartz or plagioclase. Furthermore, biotites from the Poimena and Little Mount Horror plutons have typically higher Mg# and TiO_2 (2.88–5.55%)(Groves 1977, McClenaghan & Williams 1982). Elsewhere in eastern Tasmania, some alkali feldspar granites contain very iron-rich, low Ti biotites, but these have generally lower tetrahedral Al and contain much more F (0.6–4.2%) (Groves 1977, J. L. Everard unpublished data).

TABLE 6
Representative mineral analyses: biotite

Sample	CPJ32	PHS	CPJ32	CPJ32	CPJ33	PHN
Analysis	R2	R3/1	R3/3	R6/9	R1/2	R5/3
Type	pheno	pheno	rim on mt	rim on fa	incl in mt	gmass
SiO_2	33.24	32.70	33.01	33.01	32.82	32.31
TiO_2	1.66	1.30	0.69	0.35	1.81	0.65
ZrO_2	na	na	0.02	0.08	na	0.03
Al_2O_3	14.44	13.98	11.79	10.32	10.13	11.45
Cr_2O_3	–	0.02	na	na	–	0.02
V_2O_3	0.02	–	na	na	–	na
FeO_t	33.08	36.68	38.84	38.19	40.83	36.99
MnO	0.30	0.51	0.69	1.01	0.54	0.60
ZnO	0.12	0.14	na	na	0.02	na
NiO	0.07	–	na	na	na	–
MgO	4.12	1.89	1.10	1.85	0.16	2.06
CaO	–	0.02	0.04	0.14	0.07	0.08
Na_2O	0.70	0.61	0.75	0.54	0.24	0.43
K_2O	8.46	7.67	7.95	7.71	7.75	7.67
SrO	–	0.08	na	na	–	na
BaO	0.65	0.47	na	na	–	na
F	0.08	0.09	0.01	0.08	0.14	0.15
Cl	0.13	0.11	0.04	0.04	0.01	0.08
O=(F,Cl)	–0.06	–0.06	–0.05	–0.05	–0.06	–0.08
Total	97.06	96.21	95.05	93.28	94.48	92.44
atoms on the basis of (O) = 20, (OH, F, Cl) = 4						
Si	5.414	5.456	5.660	5.764	5.712	5.650
Al^{iv}	2.586	2.544	2.340	2.123	2.079	2.350
Al^{vi}	0.186	0.205	0.037	–	–	0.011
Cr	–	0.002	na	na	–	0.003
V	0.002	–	na	na	–	na
Ti	0.204	0.163	0.089	0.046	0.237	0.085
Zr	na	na	0.001	0.006	na	0.002
Fe as Fe^{II}	4.506	5.118	5.554	5.576	5.944	5.410
Mn	0.041	0.073	0.010	0.149	0.080	0.088
Zn	0.014	0.017	na	na	0.003	na
Ni	0.009	–	na	na	na	–
Mg	1.001	0.470	0.281	0.482	0.042	0.537
Ca	–	0.004	0.008	0.026	0.013	0.015
Na	0.222	0.198	0.247	0.183	0.081	0.146
K	1.758	1.633	1.735	1.716	1.721	1.712
Sr	–	0.008	na	na	–	na
Ba	0.042	0.031	na	na	–	na
F	0.042	0.047	0.053	0.047	0.076	0.085
Cl	0.035	0.032	0.011	0.013	0.004	0.022
(OH)	3.923	3.922	3.936	3.940	3.920	3.893
cation total	15.985	15.920	16.052	16.071	15.912	16.009
Mg#	18.18	8.41	4.82	7.95	0.70	9.03

na – not analysed; pheno – phenocryst; incl – inclusion; gmass – groundmass; mt – magnetite; fa – fayalite.

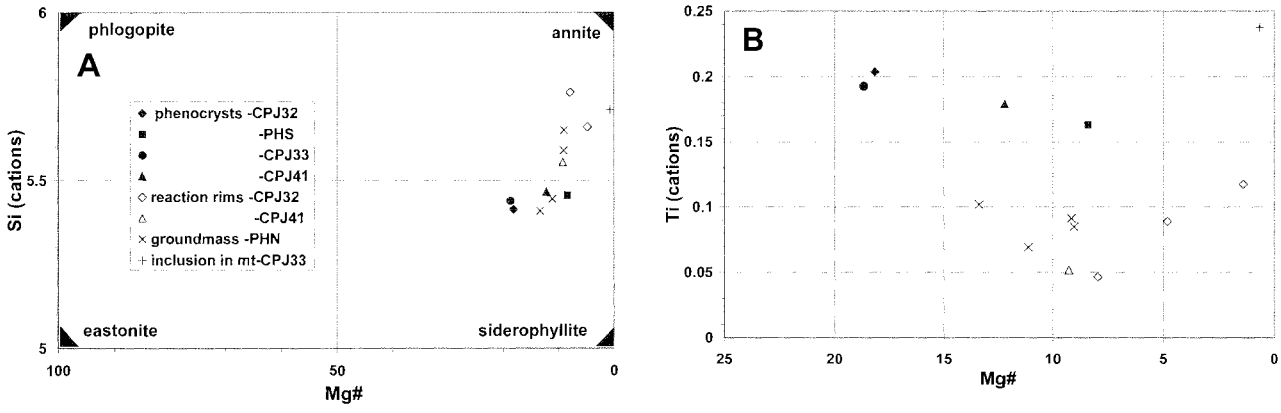

FIG. 5 — Electron microprobe analyses of biotite. (A) Si cations against Mg#, ideal end-member compositions also shown. (B) Ti cations against Mg#.

The biotite microphenocrysts are probably cognate products of fractionating phonolitic magma at depth, and disequilibrium at emplacement may be due to lower pressure. In some samples, biotite re-appeared later as a groundmass phase, probably because crystallisation of sodic amphiboles and pyroxenes had increased K/Na in the residual liquid just prior to solidification.

Feldspars

Both X-ray diffraction and electron microprobe data indicate that two alkali felspars (sanidine and anorthoclase) are present. Simple Carlsbad twinning is ubiquitous and very fine, multiple twinning common, but cross-hatched twinning was not observed. Undulose extinction indicating compositional zoning is common. In some samples, feldspar is turbid and partly altered to fine-grained sericite (pl. 3).

Most of the analysed feldspars (table 7, fig. 6) are anorthoclase ($Or_{10.0\text{-}37.6}$) with small amounts of CaO (up to 8.6 mole % anorthite in solid solution). Some have significant BaO (≤2.51%) and SrO (≤1.31%), corresponding to 4.5 mole % celsian (Ba-feldspar) and 3.4 mole % Sr-feldspar, respectively. The remaining analyses are sanidine ($Or_{62.8\text{-}91.1}$) with very low CaO, BaO and SrO. All analyses contain minor iron (0.15 - 0.31 % as FeO).

The groundmass of CPJ41 contains small grains of near-stoichiometric celsian, and a grain intermediate between celsian and K-feldspar. Celsian is rare in igneous rocks, and mostly occurs in hydrothermal or contact-metamorphic manganese deposits. Here, it is probably a very late-stage deuteric mineral. Some feldspars plot very close to the albite or K-feldspar end-members, but the analyses are less satisfactory, with high totals and/or significant cation deficiencies. These may have crystallised or been altered during late-stage hydrothermal processes.

Pyroxenes

Small, well-formed, elongate to acicular prisms (typically 20 –100 to rarely 400 µm long x 5–20 µm across) of pale yellow to green clinopyroxene are abundant (pl. 6). Analyses (table 8) are recalculated to four cations and Fe distributed to Fe^{III} and Fe^{II} to ensure charge balance (6 oxygens). Although all these pyroxenes are iron-rich with low TiO_2 (≤0.43%) and little or no tetrahedrally coordinated Al, they fall into two groups. The nomenclature follows Morimoto (1988).

Those from CPJ32, and a few from PHN and CPJ33, are relatively calcic (CaO 13.06–19.27%) and are hedenbergites or relatively calcic aegirine-augites (fig. 7). In CPJ32, their pleochroism is α deep green, β pale yellow-green, γ pale yellow-brown.

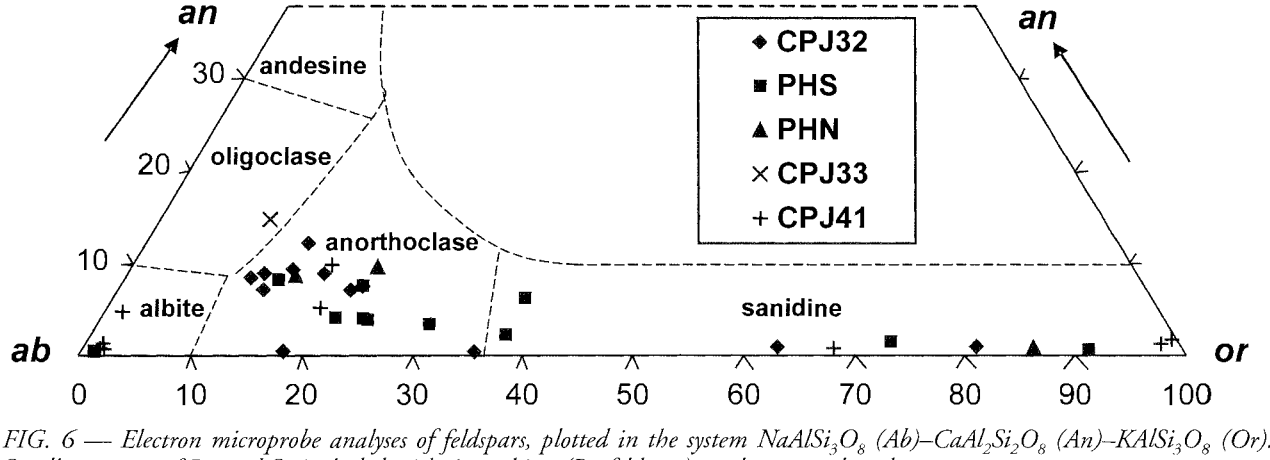

FIG. 6 — Electron microprobe analyses of feldspars, plotted in the system $NaAlSi_3O_8$ (Ab)–$CaAl_2Si_2O_8$ (An)–$KAlSi_3O_8$ (Or). Small amounts of Ba and Sr included with An; celsian (Ba feldspar) analyses not plotted.

TABLE 7
Representative mineral analyses: feldspars, feldspathoids and analcime

Sample	CPJ32	PHS	PHN	CPJ32	PHS	PHN	CPJ41	CPJ32	PHS	CPJ33
Analysis	R1/4	R11/2	R4/3	R9/a	R8/1	R6/7	e1	R11/5	R12/4	R1/6
mineral	anorthoclase			sanidine			celsian	nepheline	sodalite	analcime
SiO_2	66.04	64.18	63.71	65.52	63.96	63.75	31.50	43.39	37.41	56.57
TiO_2	0.02	0.02	–	0.02	–	–	–	–	–	–
Al_2O_3	21.65	19.81	20.03	19.55	18.95	18.29	25.98	32.60	31.49	23.12
FeO	0.28	0.24	0.27	0.15	0.31	0.11	0.25	0.18	0.23	0.06
MgO	–	–	–	–	–	–	0.01	–	–	0.02
CaO	1.28	0.45	0.56	0.05	–	–	0.19	–	0.00	–
Na_2O	8.47	6.46	7.71	4.15	0.98	1.51	0.10	14.89	24.54	13.01
K_2O	2.03	6.46	3.81	10.79	15.69	14.60	0.05	6.48	0.10	0.08
P_2O_5	–	na	na	0.02	–	na	na	na	na	na
SrO	–	0.40	0.76	0.01	–	–	0.04	–	–	–
BaO	1.02	1.48	2.51	0.13	0.13	0.28	40.00	0.01	0.05	–
SO_3	na	na	na	na	na	na	na	na	0.40	na
Cl	–	na	na	–	0.06	na	na	na	6.86	na
O=Cl	–	na	na	–	–0.01	na	na	na	–1.55	na
TOTAL	100.80	99.49	99.36	100.39	100.06	98.53	98.11	97.55	99.55	92.87
atoms on the basis of (O) =										
	8	8	8	8	8	8	8	4	12.5	6
Si	2.911	2.929	2.913	2.964	2.963	2.986	2.013	1.064	3.026	2.035
Ti	0.001	0.001	–	0.001	–	–	–	–	–	–
Al	1.125	1.066	1.079	1.043	1.035	1.001	1.957	0.942	3.001	0.980
Fe	0.010	0.009	0.010	0.006	0.012	0.004	0.013	0.004	0.015	0.002
Mg	–	–	–	–	–	–	0.001	–	–	0.001
Ca	0.061	0.022	0.028	0.002	–	–	0.013	–	0.001	–
Na	0.724	0.571	0.683	0.364	0.088	0.137	0.012	0.708	3.848	0.907
K	0.114	0.376	0.222	0.623	0.927	0.872	0.004	0.203	0.011	0.004
Sr	–	0.011	0.020	–	–	–	0.001	–	–	–
Ba	0.018	0.026	0.045	0.002	0.002	0.005	1.002	–	0.002	–
P	–	na	na	0.001	–	na	na	na	na	na
S	na	na	na	na	na	na	na	na	0.024	na
Cl	–	na	na	–	0.004	na	na	na	0.940	na
cation total	4.963	5.011	5.000	5.006	5.027	5.014	5.017	2.920	9.903	3.930
end-members (mole %)										
an	6.6	2.2	2.8	0.2	–	–	1.2	ne 71.7		
ab	79.0	56.8	68.4	36.7	8.6	13.5	1.2	ks 20.5		
or	12.4	37.4	22.3	62.8	91.1	86.0	0.4	Q 7.8		
Sr feldspar	–	1.1	2.0	–	–	–	0.1			
celsian	1.9	2.6	4.5	0.2	0.2	0.5	97.0			

TABLE 8
Representative mineral analyses: pyroxenes

Sample	CPJ32	PHN	PHN	CPJ33	PHS	CPJ33
Analysis	R6/1	R7/2	R4/5	R7/3	R2/3	R2/4
Mineral	Hedenbergite		Aegirine-augite		Aegirine	
SiO_2	46.90	48.05	49.35	50.64	52.05	51.49
TiO_2	0.32	0.12	0.16	0.41	0.20	0.34
ZrO_2	0.35	0.28	0.51	1.19	0.46	2.11
Al_2O_3	1.99	1.42	2.23	1.20	3.88	1.03
Cr_2O_3	0.03	-	0.02	-	0.01	-
FeO_t	24.72	24.90	26.58	27.70	25.38	27.57
MnO	1.02	1.03	0.90	0.63	0.57	0.32
NiO	-	0.03	-	-	-	0.04
MgO	1.75	2.14	0.50	0.01	0.17	0.29
CaO	19.01	19.15	13.16	6.56	2.19	2.92
Na_2O	2.21	2.06	5.59	9.37	12.01	11.40
K_2O	0.15	0.02	0.02	-	0.05	0.03
Total	98.54	99.19	99.00	97.79	96.98	97.55
Cations calculated on the basis of Z = 4, (O) = 6						
Si	1.899	1.934	1.953	1.986	1.989	1.998
Al^{iv}	0.095	0.066	0.047	0.014	0.011	0.002
Al^{vi}	-	0.001	0.057	0.042	0.164	0.046
Ti	0.001	0.004	0.005	0.012	0.006	0.001
Zr	0.007	0.006	0.001	0.023	0.009	0.040
Cr	0.001	-	0.001	-	0.000	-
Fe^{III}	0.253	0.209	0.389	0.615	0.711	0.716
Fe^{II}	0.584	0.629	0.491	0.293	0.100	0.179
Mn	0.035	0.035	0.030	0.021	0.018	0.011
Ni	-	0.001	-	-	-	0.001
Mg	0.105	0.128	0.029	0.006	0.001	0.017
Ca	0.829	0.826	0.558	0.276	0.090	0.122
Na	0.174	0.161	0.429	0.713	0.890	0.858
K	0.008	0.001	0.000	-	0.002	0.001
Mg#	15.30	16.92	5.64	1.90	9.01	8.66

The remaining analyses, including all from PHN and CPJ41, are sodic pyroxenes with low CaO (≤7.12%). Most are aegirines, but a few are sodic aegirine-augites. Crystallographic orientation is difficult due to the small grain size, but in PHS pleochroism is approximately α pale green, β and γ pale greenish yellow.

MnO (≤1.19%) ranges to higher values in hedenbergite and calcic aegirine-augite, whereas Al_2O_3 (1.03–3.88%) ranges higher in aegirine, implying some solid solution towards jadeite. ZrO_2 is variable but sometimes relatively high (0.28–0.54% in hedenbergite, 0.10–2.11% in aegirine) and does not correlate with other elements, grain size or morphology.

An apparent slight excess of Si (≤2.027 cations per formula unit) in some aegirine analyses may result from small amounts of unanalysed elements. In particular, Nb is relatively high in the whole rock (169–174 ppm, see below) and can enter sodic pyroxenes, as Nickel & Mark (1965) report 1.04% Nb_2O_5 in aegirine-augite (and 0.14% in arfvedsonite) in a paragneiss at Seal Lake, Labrador.

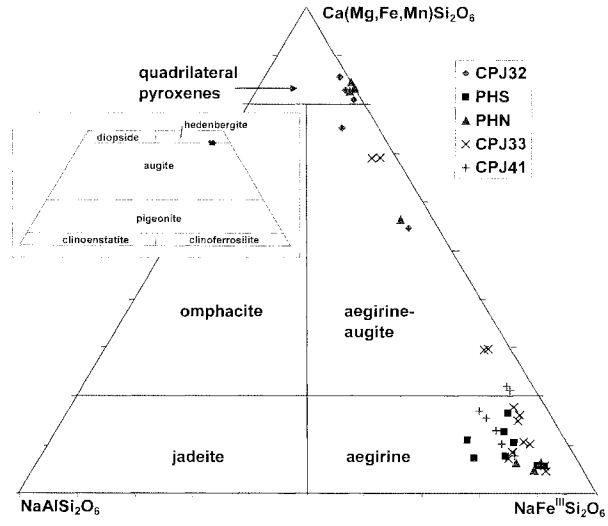

FIG. 7 — Electron microprobe analyses of pyroxenes projected on to the plane $NaAlSi_2O_6$ (jadeite)–$NaFe^{III}Si_2O_6$ (acmite)–$Ca(Mg,Fe,Mn)Si_2O_6$ (quadrilateral clinopyroxene). Inset shows hedenbergites plotted on to the pyroxene quadrilateral (diopside-hedenbergite-clinoenstatite-clinoferrosilite). Nomenclature after Morimoto (1988).

Amphiboles

Sodic amphibole is common in the groundmass as ragged prisms (mostly ≤100 μm long) (pl. 5) and more rarely as subhedral to euhedral pseudohexagonal sections (≤200 μm across) (pl. 6) or glomerocrystic clots. In PHS, an amphibole rhomb (200 x 100 μm) encloses a fayalite grain (70 μm).

Analyses (table 9) were converted to the amphibole formula $AB_2C_5T_8O_{22}(OH,F,Cl)_2$ by the method of J. C. Schumacher (in Leake 1997, appendix 2). For all of these amphiboles, estimates of minimum Fe^{III} are given by the "16CAT" formulae, in which the cations are recalculated to sum to 16, implying full occupancy of the A sites, and Fe distributed between Fe^{III} and Fe^{II} to maintain charge balance. They fall into two distinct populations.

Those from CPJ32 and a few from CPJ33 are iron-rich calcic amphiboles with substantial substitution of Al for Si in the tetrahedral (T) sites. They also have low $Mg/(Mg+Fe^{II})$, and since Fe^{III} > Al in the C sites most fall into the hastingsite field (fig. 8). Analysis R7/5 falls into the ferroedenite field because of its slightly higher Si. Optically, the hastingsite in CPJ32 is length slow with distinctive pleochroism (α pale straw yellow-brown, β deep khaki green to olive-green, γ blue-green).

The remaining analyses, including all those from PHS, PHN and CPJ41, have much higher SiO_2 and Na_2O and very low Al_2O_3 and CaO. They are sodic amphiboles, because the B sites are largely occupied by Na. Because of their low tetrahedral Al and high $Mg/Mg+Fe^{II}$ and Fe^{III} relative to octahedral Al, they are classified as arfvedsonite (fig. 8), and several lie close to the end-member $(Na,K).Na_2.Fe_4^{II}Fe^{III}.Si_8O_{22}(OH,F)_2$. Optically, the arfvedsonite in PHS is length fast and strongly coloured (α very dark blue-green, β pale greenish- to olive-brown, γ dark grey-green).

TABLE 9
Representative mineral analyses: amphiboles

Sample		CPJ32	CPJ33	CPJ32	PHS	CPJ33	CPJ41
Analysis		R2/3	R4/1	R7/5	R7/2	R2/2	R1/7
Mineral		Hastingsite		Edenite	Arfvedsonite		
SiO_2		38.66	39.05	40.58	49.03	48.19	47.94
TiO_2		0.67	0.69	0.52	0.04	0.51	0.14
ZrO_2		0.28	0.52	0.33	0.04	0.13	2.08
Al_2O_3		9.11	8.43	8.09	1.04	1.45	1.77
Cr_2O_3		0.04	0.01	-	0.04	-	0.04
FeO		30.49	32.18	31.05	31.87	32.17	32.69
MnO		0.77	0.74	0.78	1.83	1.68	1.64
NiO		-	-	-	-	-	0.03
MgO		2.47	1.61	1.91	2.21	0.87	0.73
CaO		9.96	9.97	8.84	1.29	0.76	0.83
SrO		-	-	-	0.21	-	0.06
Na_2O		3.18	3.21	3.51	6.57	7.70	7.56
K_2O		1.24	1.42	1.44	2.92	2.07	2.15
BaO		-	-	0.09	-	-	0.04
F		0.07	0.09	0.07	0.23	0.22	0.25
Cl		0.06	0.05	0.06	-	0.02	0.01
O=(F,Cl)		-0.04	-0.05	-0.04	-0.01	-0.01	-0.11
Total		96.96	97.93	97.24	97.23	95.67	97.86
atoms on the basis of $AB_2C_5T_8O_{22}(OH,F)_2$ (16CAT formulae)							
Si	T	6.291	6.348	6.605	7.859	7.841	7.720
Al^{iv}	T	1.709	1.615	1.395	0.141	0.159	0.280
Al^{vi}	C	0.038	-	0.156	0.056	0.119	0.056
Cr	C	0.005	0.002	-	0.005	-	0.005
Ti	C	0.082	0.084	0.064	0.005	0.063	0.017
Zr	C	0.022	0.041	0.026	0.003	0.010	0.164
Fe^{III}	C	0.720	0.744	0.466	0.704	0.752	0.659
Fe^{II}	C	3.429	3.630	3.761	3.568	3.624	3.744
Ni	C	-	-	-	-	-	0.004
Mg	C	0.600	0.390	0.464	0.529	0.212	0.176
Mn	C	0.104	0.102	0.063	0.130	0.221	0.176
Mn	B	0.002	-	0.045	0.119	0.011	0.048
Ca	B	1.736	1.737	1.542	0.222	0.132	0.143
Sr	B	-	-	-	0.020	-	0.005
Na	B	0.262	0.307	0.413	1.640	1.857	1.804
Na	A	0.742	0.705	0.695	0.402	0.571	0.555
K	A	0.258	0.295	0.299	0.598	0.429	0.442
Ba	A	-	-	0.006	-	-	0.002
F		0.035	0.045	0.037	0.116	0.113	0.129
Cl		0.016	0.015	0.015	-	0.005	0.003
OH		1.949	1.941	1.957	1.884	1.883	1.868
Mg#		14.89	9.70	10.98	12.91	5.52	4.49

Arfvedsonite is lower in TiO_2 and higher in MnO (≤2.95%) and K_2O (≤3.10%) than hastingsite. All are low in Ba, Sr, F (≤0.25%) and Cl (≤0.06%). As in pyroxenes, ZrO_2 is very variable but sometimes considerable (up to 2.08% in arfvedsonite).

For some analyses, the total occupancy of the T and C sites is slightly less than 13, due to an excess of cations that must be allocated to the A and B sites (i.e., Ca, Na, Ba and Sr) relative to all other cations. This cannot be corrected by any assumption regarding Fe^{III}/Fe^{II}, and suggests an analytical problem. It is possible that there are small amounts of additional, unanalysed elements in the C sites, particularly REE or Nb.

The formulae can be projected on to a ternary diagram (fig. 8) depicting the three mutually coupled substitutions Si ↔ Al in the T sites, (Mg, Fe^{II}, Mn) ↔ (Al, Fe^{III}) in the C sites, and Na ↔ Ca in the B sites. The amphiboles lie fairly close to the end members of the join between hastingsite/pargasite and arfvedsonite/eckermannite, in which the first and third of the above substitutions are coupled.

Apatite

Accessory apatite is present as small laths (≤250 x 20 μm), acicular prisms (pl. 6) and hexagonal cross-sections (rarely ≤100 μm but mostly ≤15 μm) in the groundmass and as inclusions in fayalite and magnetite microphenocrysts.

Typical analyses (table 10) are near-stoichiometric, with mostly small amounts of iron (≤1.29% as FeO), SrO (≤0.94%), BaO (≤0.96%), Na_2O (≤0.53%) and light rare earth elements (LREE) (≤1.65% La_2O_3 + Ce_2O_3). They are relatively low in F (one analysis 1.88%, rest ≤ 1.18%) and Cl (≤0.37%) and are mostly hydroxyapatites.

Small apatite grains from CPJ41 and PHS, however, have large amounts of SrO (≤25.74%) and LREE (≤12.22%). In CPJ41 they accompany celsian and may be a late stage hydrothermal mineral.

Nepheline, Sodalite and Analcime

The feldspathoidal material consists of an irregularly polygonal aggregate of colourless anhedra, each typically 25–150 μm across. Some is weakly birefringent and sometimes slightly turbid, and has optical properties consistent with nepheline. The remainder, with slightly higher relief, is clear and isotropic (pl. 3), and probably consists of sodalite and analcime, as indicated by X-ray diffraction. The more altered samples (CPJ33, PHN) lack nepheline and sodalite, and analcime is more abundant.

Because of their fine grain size, "clean" near-stoichiometric microprobe analyses of these minerals (table 7) were difficult to obtain, and some are probably mixtures of two or more Na-Al silicates and other minerals. In addition, the analyses are usually deficient in Na relative to the ideal formulae, probably due to volatilisation in the electron beam. Small amounts of iron (usually <0.5% as FeO) are invariably present.

Reasonably stoichiometric analyses of nepheline were obtained from CPJ32, PHS and CPJ41. They contain appreciable K_2O (4.67–6.69%) suggesting approximately 15–20 mole % $KAlSiO_4$ in solid solution, and "excess silica" corresponding to 10–15% solid solution towards alkali feldspar. Near-stoichiometric sodalite ($Na_4Al_3Si_3O_8Cl$) was

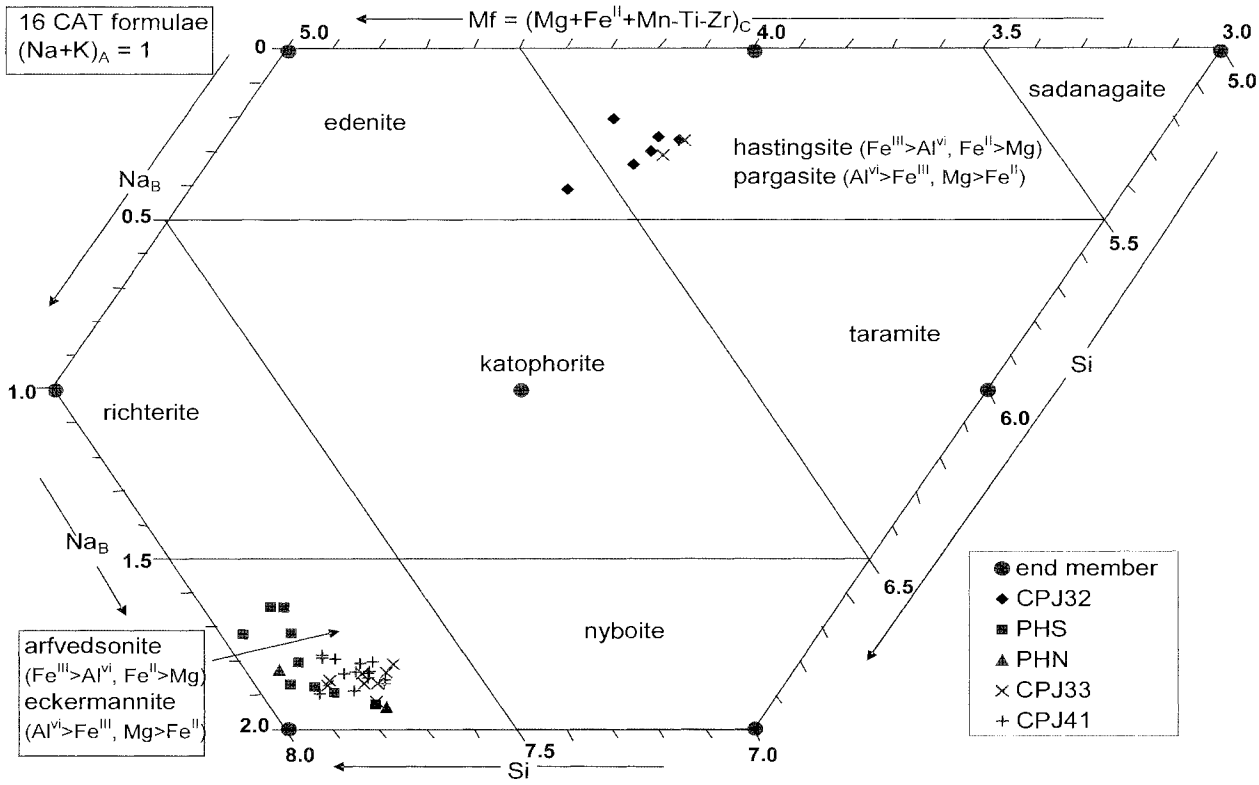

FIG. 8 — Electron microprobe analyses of amphiboles (16 CAT, minimum Fe^{III} formulae) projected on to the system edenite-richterite-arfvedsonite/eckermannite-nyboite-taramite-hastingsite/pargasite, showing coupled substitutions and ideal end-member compositions. Nomenclature consistent with Leake et al. *(1997). See text for further discussion.*

analysed from CPJ32 and PHS. In contrast to nepheline, K_2O is negligible.

Possible analcime analyses, from four samples, are mostly less stoichiometric. Those from CPJ32 and PHS contain significant iron and/or K_2O, and some have excess alkalis suggesting contamination by sodalite.

DISCUSSION

Phenocrysts

The rare fayalite, biotite and magnetite phenocrysts probably represent near-liquidus phases that crystallised from the phonolitic magma at depth. They may have buffered fO_2 by reactions of the form

$$[1a]\ 3Fe_2SiO_4 + O_2 = 2Fe_3O_4 + 3SiO_2$$

This is the well-known quartz-fayalite-magnetite buffer, but its T-fO_2 calibration is not directly applicable, as SiO_2 is a low-activity component in the melt, rather than a mineral phase. Alternatively, it could be rewritten as

$$[1b]\ 6Fe_2SiO_4 + 3(Na,K)AlSiO_4 + 2O_2 = 4Fe_3O_4 + 3(Na,K)AlSi_3O_8$$

where nepheline, kalsilite (K-nepheline) and probably alkali feldspar are components in the melt, rather than mineral phases. Although alkali feldspar occurs as phenocrysts in the phonolite, they grade down into the groundmass and probably crystallised later than the other phenocrysts.

The strong resorption of biotite and fayalite phenocrysts may in part be due to adiabatic decompression, but the general absence of these minerals in the groundmass suggests that they were not stable at the lower pressures and temperatures during final emplacement and cooling of the dyke. Fayalite and magnetite are frequently surrounded by a reaction rim of biotite, which may be represented by reactions of the form:

$$[2a]\ 6Fe_2SiO_4 + 4KAlSiO_4 + 2SiO_2 + 4H_2O = 4KFe^{II}{}_3AlSi_3O_{10}(OH)_2$$

$$[3a]\ 2Fe_3O_4 + 2KAlSiO_4 + 4SiO_2 + 2H_2O = 2KFe^{II}{}_3AlSi_3O_{10}(OH)_2 + O_2$$

or

$$[2b]\ 6\ Fe_2SiO_4 + 3KAlSiO_4 + KAlSi_3O_8 + 4H_2O = 4KFe^{II}{}_3AlSi_3O_{10}(OH)_2$$

$$[3b]\ 2Fe_3O_4 + 2KAlSi_3O_8 + 2H_2O = 2KFe^{II}{}_3AlSi_3O_{10}(OH)_2 + O_2$$

It is clear from reactions [2] and [3], which intersect with [1] (fig. 9), that increasing fH_2O (or decreasing temperature) will favour biotite relative to fayalite and magnetite respectively. From [3], lower fO_2 will also favour biotite relative to magnetite. The experiments of Wones & Eugster (1965) place [3b] for pure annite (Fe-biotite) at about 680° C at 103.5 MPa, or about 710°C at 207 MPa, for oxygen fugacities controlled by the quartz-fayalite-magnetite buffer [1a].

TABLE 10
Representative mineral analyses: apatite

Sample	CPJ41	CPJ41
Analysis	a5	a7
SiO_2	0.33	2.79
ThO_2	0.01	0.68
La_2O_3	0.40	5.02
Ce_2O_3	0.64	5.92
Pr_2O_3	0.13	0.37
Nd_2O_3	0.24	0.91
Sm_2O_3	–	0.02
Y_2O_3	0.08	0.04
FeO	0.46	0.65
MnO	0.15	0.19
MgO	0.02	0.01
CaO	52.72	20.52
SrO	1.16	25.74
BaO	–	0.81
Na_2O	0.27	0.64
P_2O_5	40.62	31.70
As_2O_5	0.04	0.01
SO_3	0.01	0.02
F	1.03	2.03
Cl	0.32	0.01
O = (F, Cl)	–0.51	–0.86
TOTAL	98.13	97.23
Atoms on the basis of (O) = 12, (OH,F,Cl) = 1		
P	2.954	2.838
As	0.002	0.001
S	0.001	0.001
Si	0.028	0.296
Th	–	0.016
La	0.013	0.196
Ce	0.020	0.229
Pr	0.004	0.014
Nd	0.008	0.035
Sm	–	0.001
Y	0.003	0.002
Fe^{II}	0.033	0.057
Mn	0.011	0.017
Mg	0.002	0.001
Ca	4.852	2.324
Sr	0.058	1.578
Ba	–	0.034
Na	0.045	0.131
F	0.279	0.678
Cl	0.047	0.003
(OH)	0.674	0.319
cation total	8.034	7.771

Groundmass

Fergusson (1978) noted that a compositional gap occurs between Ca- and Na- rich pyroxenes within single samples of many felsic alkaline rocks, and attributed this to crystallisation of amphibole, particularly in slowly cooled intrusive rocks. In the Tomahawk phonolite, most pyroxenes are either hedenbergite or aegirine, but the analyses (fig. 7) do not show a clear compositional gap. Those in PHN and CPJ33 have a wide range with some intermediate compositions (aegirine-augite). As both pyroxene and amphibole are groundmass phases, they probably crystallised together rapidly.

However, a large and obvious compositional gap lies between Ca-rich and Na-rich amphiboles (hastingsite and arfvedsonite), even within a thin section (CPJ33; fig. 8). Intermediate sodic-calcic amphiboles near katophorite $Na_A.Na_BCa(Mg,Fe^{II})_4(Al,Fe^{III}).AlSi_7O_{22}(OH,F,Cl)_2$, on the hastingsite-arfvedsonite compositional join, are absent. Katophorite, which contains both Na and Ca in the B sites, is a comparatively rare high temperature amphibole mainly occurring in ultramafic alkaline rocks (Deer *et al.* 1997). There may be a miscibility gap between hastingsite and arfvedsonite at the lower temperatures at which the phonolite groundmass crystallised. As the remaining melt cooled and became further depleted in CaO, this solvus may have been intersected, causing the precipitating amphibole to change suddenly from hastingsite to arfvedsonite.

Arfvedsonite and aegirine may be related by reactions of the form

$$[4]\ 5NaFe^{III}Si_2O_6 + H_2O = Na_3Fe^{II}_4Fe^{III}Si_8O_{22}(OH)_2 + Na_2Si_2O_5 + O_2$$

$$[5]\ 18NaFe^{III}Si_2O_6 + 4Fe_3O_4 + 12SiO_2 + 6H_2O = 6Na_3Fe^{II}_4Fe^{III}Si_8O_{22}(OH)_2 + 5O_2$$

where SiO_2 and $Na_2Si_2O_5$ are components in the melt, the latter expressing peralkalinity.

These reactions probably intersect (fig. 9) and define a restricted sector in fO_2-fH_2O space in which both arfvedsonite and aegirine are stable, and magnetite is absent. Clearly, the reduced hydrous phase arfvedsonite is favoured by low fO_2 and high fH_2O (or lower temperature), whereas aegirine is favoured by high fO_2 and low fH_2O.

Marsh (1975) suggested that the stability of acmite (end-member aegirine) in strongly undersaturated liquids is limited by the reaction

$$[6]\ 12NaFe^{III}Si_2O_6 = 4Fe_3O_4 + 6Na_2Si_2O_5 + 12SiO_2 + O_2$$

for which thermodynamic calculations suggested unrealistically high oxygen fugacities (above the hematite-magnetite buffer). This is contrary to petrographic evidence in some nepheline syenites (and the Tomahawk phonolite) and was attributed to inaccurate thermodynamic data (specifically, the free energy of acmite).

Aenigmatite ($Na_2Fe^{II}_5TiSi_6O_{20}$) is common in many peralkaline phonolites and its absence in the Tomahawk River dyke requires comment. Marsh (1975) noted that it typically forms by the reaction of Ti-magnetite with a peralkaline undersaturated liquid. Because of inadequate thermodynamic data he could not define its stability field, but suggested that it lay at low fO_2 and was enlarged by high activity of $Na_2Si_2O_5$ (in melt) and low activity of $NaFeSi_2O_6$ (in pyroxene). High fO_2 and/or aegirine-rich

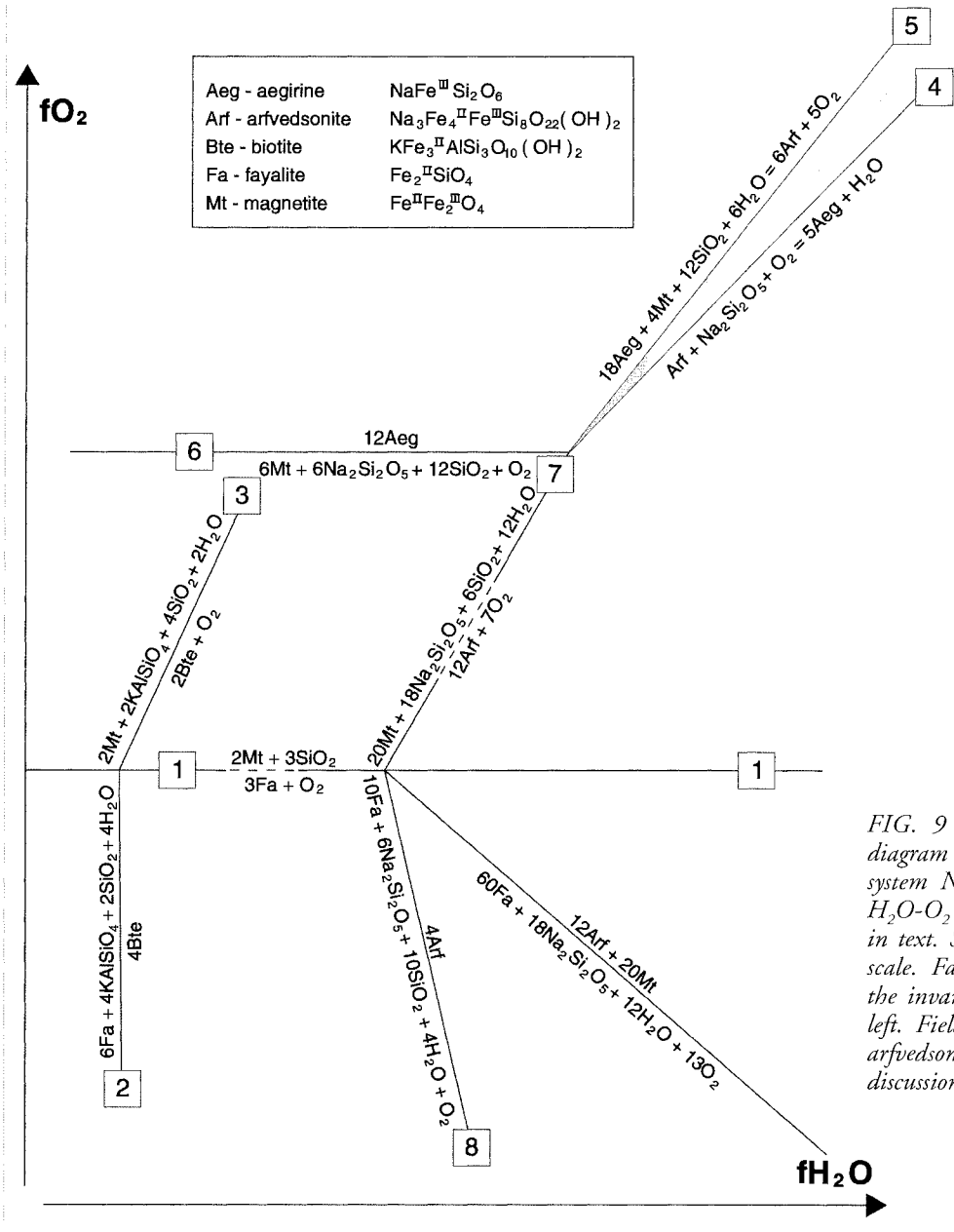

FIG. 9 — Partial Schreinemakers diagram (fO_2-fH_2O, isothermal) for the system Na_2O-(K_2O-Al_2O_3)-FeO-SiO_2-H_2O-O_2 showing reactions mentioned in text. Schematic only with arbitrary scale. Falling temperature will move the invariant points down and to the left. Field of co-existing aegirine and arfvedsonite shaded. See text for further discussion.

pyroxene may explain the absence of aenigmatite in the Tomahawk River dyke. Alternatively, it may result from the very low TiO_2 content (0.05–0.06%, see below) of the dyke. Although low-Ti aenigmatite has been both synthesised and reported in natural rocks, its stability field is restricted to lower fO_2 and pressures than normal aenigmatite (Deer *et al.* 1997 and references therein). In this rock, reaction of magnetite with peralkaline melt instead produced rims of biotite or haloes of aegirine and arfvedsonite, by reactions [3], [6] and/or

[7] $20Fe_3O_4 + 18Na_2Si_2O_5 + 6SiO_2 + 12H_2O = 12Na_3Fe^{II}_4Fe^{III}Si_8O_{22}(OH)_2 + 7O_2$

There is also petrographic evidence (pl. 6) for direct reaction of fayalite with peralkaline melt to produce arfvedsonite:

[8] $10Fe_2SiO_4 + 6Na_2Si_2O_5 + 10SiO_2 + 4H_2O + O_2 = 4Na_3Fe^{II}_4Fe^{III}Si_8O_{22}(OH)_2$

WHOLE ROCK CHEMISTRY

Analytical Techniques

Two fresh samples, CPJ32 and PHS, were crushed in a steel jaw crusher. Major elements were determined by X-ray fluorescence (XRF) on glass discs, prepared by standard techniques at Mineral Resources Tasmania (MRT) laboratories, Hobart. FeO/Fe_2O_3 was determined by titration and CO_2 by gravimetric methods. H_2O+ was calculated from loss-on-ignition after adjusting for FeO, CO_2 and SO_3.

Four separate determinations were made of many trace elements. XRF analyses, using standard techniques on pressed pellets, were done at both MRT and the University of Tasmania. Each sample was also analysed by inductively coupled plasma mass spectroscopy (ICP-MS) at the University. Small (5–10 mm) chips remaining from the initial jaw crushing were ground in agate and digested by two techniques: HF-HNO_3 digestion in Savillex® teflon vessels on a hotplate at 130°–150°C and 1 atmosphere, and

the PicoTrace® HF/H_2SO_4–$HClO_4$ digestion system at ≤2000 kPa and ≤180°C. Full details of procedures are given by Yu *et al.* (2001) and data by Everard (2004).

Although the ICP-MS data mostly have better precision and lower detection limits than XRF, errors may arise from incomplete digestion of resistant minerals. Data obtained using the more intensive PicoTrace® digestion system are generally preferred, as values for several elements (REE, Y, Zr, Hf and Sn) exceed those obtained by Savillex® digestion, but are similar to XRF data where available.

For Cr, V and Ba, the university XRF data are preferred because of contamination or digestion problems with ICP-MS. W and As were below XRF detection limits (10 ppm) at MRT. For Li and Be, which are difficult to determine, the average of two ICP-MS determinations, rounded to the nearest ppm, are quoted. The remaining trace element data in table 11 were determined by PicoTrace® digestion and ICP-MS.

Major Elements

Both analyses are phonolites according to the total alkali-silica diagram of Le Bas *et al.* (1986) (fig. 10) and the CIPW-normative classification of Johnson & Duggan (1989) (DI > 75; *An* < 50 mol %, and *ne* > 10 %).

The high (>1) Agpaitic Index (table 11) indicates a peralkaline composition (molar (Na_2O+K_2O) > molar Al_2O_3). Mineralogically, this is expressed by the presence of sodic amphiboles, sodic pyroxenes and sodalite and the absence of calcic plagioclase.

Compared with the average phonolite of Le Maitre (1976), and those in eastern Australia (table 11) and elsewhere, the Tomahawk River phonolite is exceptionally depleted in TiO_2, MgO and CaO and has unusually high Na_2O/K_2O. Of the eastern Australian examples quoted, only the Cretaceous (72 Ma) Baralaba plug (Sutherland *et al.* 1996) is also peralkaline, although less strongly so, and more depleted in MgO, CaO and also P_2O_5.

When CIPW-normative components *or*, *ab* and *ne* are calculated and plotted as weight % on to the $NaAlSiO_4$-$KAlSiO_4$-SiO_2 system (fig. 11), the analyses plot very near the feldspar-nepheline temperature minima as determined at atmospheric pressure (Schairer 1950) and 98 MPa (0.98 kb) water pressure (Hamilton & McKenzie 1965). This suggests that, like many other phonolites, compositions were largely controlled by crystal-liquid equilibrium processes at relatively low pressures. However, the minima in this system are relatively insensitive to pressure, and the Tomahawk River phonolite has other significant components, particularly the Na-bearing component *ac* (acmite) which accounts for its peralkalinity and high Na_2O/K_2O.

Bailey (1976) reviewed experimental work relevant to peralkaline feldspathoidal rocks. Although the effect of acmite (end-member aegirine) on the K-bearing system is not well determined, Schairer & Bowen (1956) found that excess Na_2O (i.e., peralkalinity) at 1 atmosphere extends the albite-nepheline cotectic from 1063°C to a eutectic with $Na_2Si_2O_5$ at 732°C. Bailey & Schairer (1966) found that the phase relations in system Na_2O-Al_2O_3-Fe_2O_3-SiO_2 at 1 atmosphere largely reflect the incongruent melting of acmite (to hematite and liquid). Crystallisation of albite, nepheline and acmite from a sodium silicate *(ns)*- normative liquid leads to a eutectic with $Na_2Si_2O_5$ at 715° ± 5°C. This matches the late groundmass crystallisation of aegirine in the Tomahawk River phonolite. Nolan (1966) found that the minimum (715°C at 98 MPa) in the join albite-nepheline-acmite coexists with magnetite and a very iron-rich liquid, but that the addition of minor diopside greatly enlarges the stability field of pyroxene.

Trace Elements

In common with most phonolites, the Tomahawk River dyke is strongly depleted in trace elements (Ni, Cr, Sc, V, Co) that are compatible in early crystallising ferromagnesian minerals. Both high field strength elements (HFSE)(Nb, Zr, La, Ce) and Rb are high, as found in many phonolites and intermediate-silicic Cainozoic and Mesozoic volcanic rocks from eastern Australia (e.g., Ewart *et al.* 1985, Sutherland *et al.* 1996).

Published analyses of phonolites (table 11 and reference list) show extreme variability in Sr (e.g., 5–3000 ppm) and Ba (e.g., 2–1645 ppm). The Tomahawk River dyke is relatively high in Sr (430, 570 ppm) and especially Ba (1040, 1300 ppm).

The chondrite-normalised REE plots (fig. 12) have distinctive concave patterns, with strong light REE (LREE) enrichment, relative middle REE (MREE) depletion, and a flat to slightly positive slope in heavy REE (HREE). Both analyses have very slight positive Eu anomalies, in contrast to the negative Eu anomaly of the Mt Wilson phonolite in Victoria (Ewart *et al.* 1985). Only a few published phonolite REE data display negative Eu anomalies, and those rocks, like the Mt Wilson phonolite, are commonly also low in Sr and Ba (e.g., Weaver 1990, Ablay *et al.* 1998). At Cantal, Massif Central (France), Wilson *et al.* (1995) distinguished aphyric "Type A" phonolites with low Sr, Ba and negative Eu anomalies from porphyritic "Type B" phonolites lacking these features.

Mantle-normalised spidergrams (fig. 13) illustrate the very strong depletions in TiO_2 and P_2O_5, whereas tetravalent trace elements (Zr, Hf, Sn) together with Pb, Mo, Sb and Li are enriched relative to comparable REE. These features presumably reflect fractionation processes rather than characteristics of the mantle source: Ti and P have clearly strongly partitioned into a fractionating phase,

---

Key to Table 11 (opposite)

[a] atomic $100Mg/(Mg+Fe^{II})$
[b] atomic $100Mg/(Mg+Fe^{total})$
[c] agpaitic (peralkaline) index: molar $(Na_2O + K_2O)/Al_2O_3$

[1] mean phonolite, n = 340 (Le Maitre, 1976)
[2] "phonolite" [trachyte], 5.92 Ma, sample 7809/3, Mt Wilson, Trentham, Vic (Ewart *et al.*, 1985)
[3] "phonolite" [trachyte], Jurassic, sample 7809/10, Coleraine, W Vic (Ewart *et al.*, 1985)
[4] phonolite, 169 Ma, sample 7809/25, Pinnacle Mt, via Mullaley, NSW (Ewart *et al.*, 1985)
[5] nepheline syenite plug, 72 Ma, Mt Ramsay, via Baralaba, Qld (Sutherland *et al.*, 1996)
[6] phonolite, <2.8 Ma, Phonolite Hill, McBride province, N Qld (Stephenson *et al.*, 1980)

TABLE 11
Whole-rock analyses

	Tomahawk River		World Av	East Australian phonolites and similar rocks				
Field No.	CPJ32	PHS	1	2	3	4	5	6
SiO_2 (%)	56.23	56.75	56.19	59.39	59.04	56.57	61.80	54.34
TiO_2	0.06	0.05	0.62	0.13	0.10	0.14	0.12	0.14
Al_2O_3	18.99	19.01	19.04	18.36	18.61	19.51	18.20	19.46
Fe_2O_3	3.27	3.86	2.79	3.78	2.67	3.54	3.10	4.15
FeO	3.01	2.24	2.03	1.93	2.57	2.34	1.10	1.55
MnO	0.19	0.20	0.17	0.13	0.19	0.17	0.14	0.17
MgO	0.26	0.17	1.07	0.35	0.31	0.37	0.10	0.98
CaO	1.01	0.83	2.72	1.25	1.36	1.72	0.50	1.89
Na_2O	10.46	10.32	7.79	7.51	6.80	8.08	8.30	8.18
K_2O	4.03	3.95	5.24	5.46	5.68	5.40	4.90	4.46
P_2O_5	0.25	0.19	0.18	0.08	0.04	0.16	0.01	0.29
SO_3	0.09	0.02	nd	nd	nd	nd	nd	nd
CO_2	0.02	0.11	0.08	-	0.19	0.27	<0.10	0.14
H_2O+	1.56	1.32	1.57	0.70	1.75	0.97	1.21	1.34
H_2O-	nd	nd	0.37	0.24	0.70	0.68	0.38	1.60
Total	99.42	99.01	99.41	99.31	100.01	99.92	99.96	98.71
FeO^{total}	5.95	5.71	4.54	5.33	4.97	5.53	3.89	5.28
Mg# [a]	13.20	11.92	48.44	24.43	17.79	21.99	13.95	52.99
mg# [b]	7.14	5.04	29.58	10.48	10.01	10.66	4.38	24.85
AI [c]	1.136	1.118	0.971	0.995	0.931	0.981	1.042	0.940
Li (ppm)	32	50						
Be	7	9						
Sc	3.99	1.26		0.97				
V	15.8	<1.5		10	15	15	2	
Cr	14.1	3.3		3	2		<10	34
Co	4.36	1.04						
Ni	7.27	0.64		4	5	3	<10	8
Cu	12.3	6.0		10	19	12	<5	13
Zn	193	219		255	148	171		125
Ga	30.2	32.4					41	27
Rb	127	131		261	241	126	195	36
Sr	572	434		41	20	129	12	848
Y	22.4	24.7		43	45	25	125	20
Zr	758	917		1710	842	932	1485	965
Nb	169	194		283	228	145	210	236
Mo	10.4	6.0						
Sn	6.13	7.20						
Sb	0.24	0.27		0.64				
Cs	3.17	3.20		8.4				
Ba	1304	1041		40	19	174	120	128
La	86.8	99.0		137			141	66
Ce	136.9	149.2		224	251	138	270	116
Pr	13.2	13.8					32	
Nd	38.9	40.2		58			94	
Sm	5.69	5.84		8.3			17	
Eu	1.82	1.78		0.85				
Gd	4.28	4.35					16	
Tb	0.70	0.72		1.12				
Dy	4.07	4.38					17	
Ho	0.81	0.87		1.44				
Er	2.39	2.65						
Tm	0.39	0.42		0.63				
Yb	2.49	2.72		4.63			5	
Lu	0.40	0.43		0.68				
Hf	14.9	17.7		36.6			18	
Ta	11.5	13.0		20.5				
Tl	0.60	0.68						
Pb	20.2	17.6		25	23	15	27	12
Bi	0.09	0.10						
Th	20.4	27.7		58	46	19	30	21
U	5.74	7.53		8.9			11	2

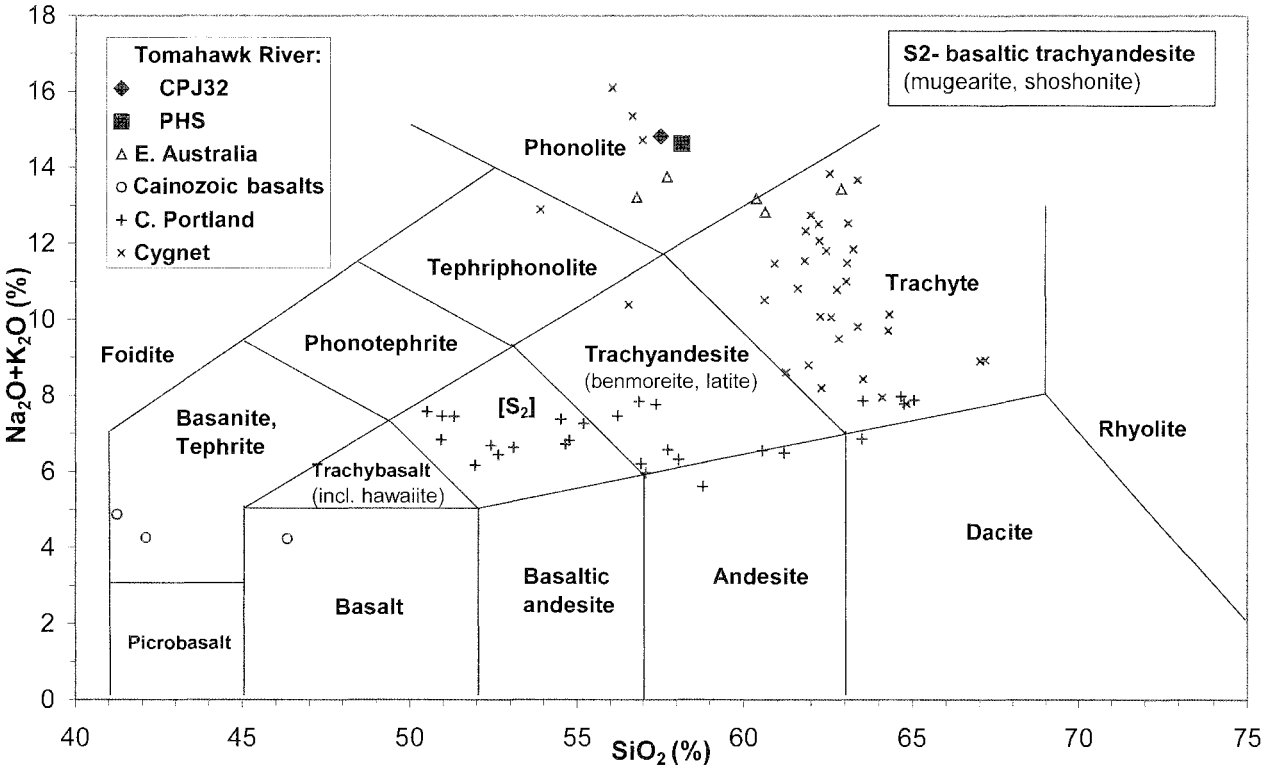

FIG. 10 — Whole-rock analyses of the Tomahawk phonolite plotted on the total alkali-silica diagram, showing volcanic rock nomenclature of Le Bas et al. *(1986). Data from other eastern Australian phonolites and trachytes (table 9), local Cainozoic basalts and Cape Portland appinites (J. L. Everard unpublished data) and Cygnet syenites (Taheri & Bottrill 1999) shown for comparison. All data recalculated to 100% anhydrous.*

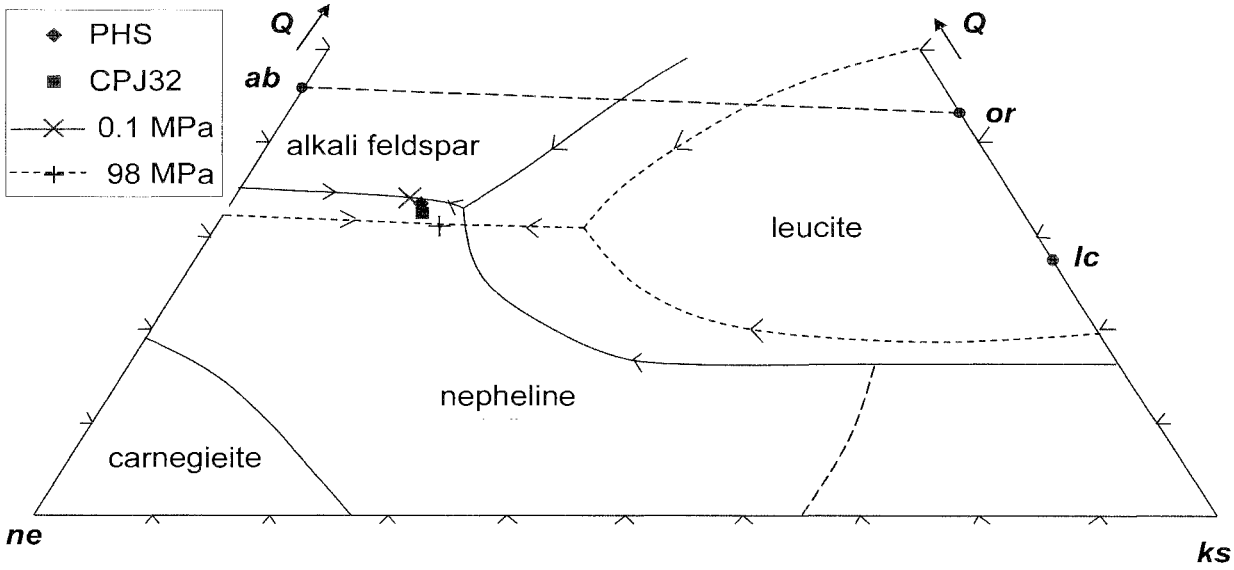

FIG. 11 — Whole-rock analyses of the Tomahawk phonolite projected on to part of the system $NaAlSiO_4$-$KAlSiO_4$-SiO_2, showing experimentally determined phase relations at 0.1 MPa (Schairer 1950) and 98 MPa (Hamilton & McKenzie 1965).

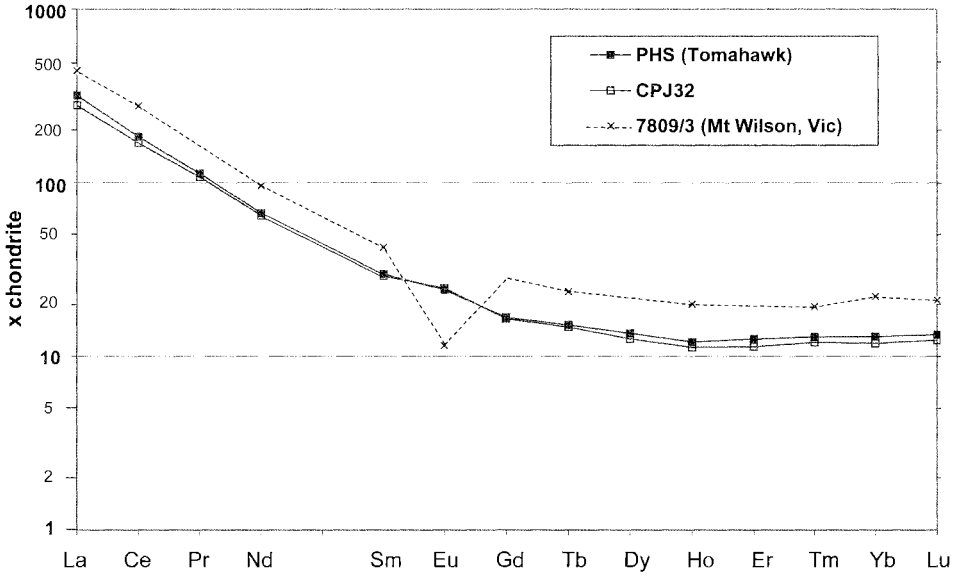

FIG. 12 — Chondrite normalized rare-earth plot for Tomahawk phonolite; data for Mt Wilson phonolite, Victoria (table 9 and Ewart et al. 1985) also plotted (with Gd interpolated) for comparison. Chondrite normalization factors after Boynton (1984).

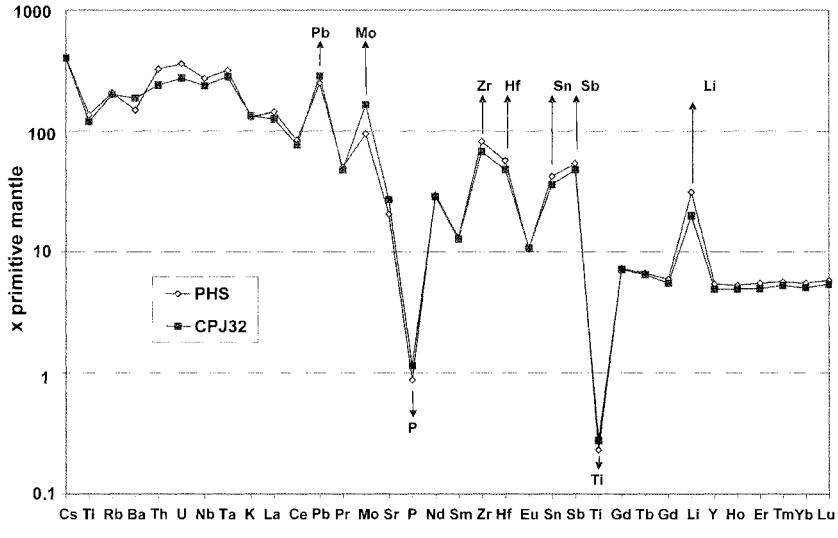

FIG. 13 — Primitive mantle (Sun & McDonough 1989) normalized trace element spider-diagram for Tomahawk phonolite analyses.

whereas REE (especially MREE and HREE) and Sr have been weakly compatible.

Although the two analyses are very similar, PHS generally has slightly lower levels of compatible trace elements (and also TiO_2, MgO and CaO) and higher levels of incompatible elements, indicating that it is more evolved than CPJ32.

Petrogenesis

Although Bailey (1974) maintained that large volumes of phonolitic magma are generated by partial melting in the lower continental crust, most workers ascribe phonolites to the extreme fractionation of silica-undersaturated mafic magmas, such as alkali basalt, basanite or nephelinite. In many studies this is supported by quantitative models of fractional crystallisation and/or direct observation of upward changes in chemical composition within a lava pile or tephra sequence (e.g., Garcia *et al.* 1986, Kyle 1981, Kyle *et al.* 1992, Le Roex 1990, Price *et al.* 1985, Thompson *et al.* 2001, Weaver 1990, Wörner & Schmincke 1984b). Wilson *et al.* (1995) and Ablay *et al.* (1998) suggested crustal assimilation combined with fractional crystallisation (AFC processes) may also occur.

Although lherzolite-bearing olivine nephelinite lavas occur 2–4 km east of the Tomahawk River dyke (Baillie *et al.* 1978, J. L. Everard, unpublished data; figs 1, 2), they are almost certainly outliers of the Miocene (16 Ma) Ringarooma volcanism (McClenaghan *et al.* 1982) and are thus unrelated. In the absence of any potentially parental mafic or intermediate rocks, a discussion of the petrogenesis of the Tomahawk River phonolite is speculative. However, some qualitative comments can be made, particularly by comparing its geochemistry with some of the above examples.

The high HFSE and Rb are generally consistent with strong crystal fractionation, but the lack of Sr or Ba depletion or negative Eu anomalies implies that neither alkali feldspar nor plagioclase were major fractionating phases. This suggests an already strongly undersaturated parental basanite or nephelinite with low normative feldspar. The very low levels of compatible elements (MgO, Ni, Cr etc.) suggest dominant olivine, pyroxene and/or amphibole fractionation left a residual felsic liquid that approached the feldspar-nepheline minimum. Strong depletion of P suggests removal of apatite, consistent with apatite inclusions in magnetite and fayalite microphenocrysts.

Fractionation of kaersutitic amphibole from a mafic precursor could account for the concave REE patterns, as MREE are strongly partitioned into amphibole (Sisson 1994), and together with titanomagnetite fractionation may partly account for Ti depletion. Additionally, as noted by Ablay *et al.* (1978), kaersutite has a low Na:Al ratio and its removal will delay feldspar crystallisation and drive the melt towards peralkaline compositions.

REGIONAL SIGNIFICANCE AND CONCLUSION

In Tasmania, the Cretaceous was mainly a prolonged period of non-deposition or erosion, and surface environments are rarely preserved. Only localised and relatively minor Cretaceous igneous rocks, mainly intrusions, are known. All are appreciably older than the phonolite, and compositionally dissimilar to it (fig. 10).

Cretaceous appinitic rocks occur in northeast Tasmania at Cape Portland, about 30 km to the northeast of Tomahawk River, as irregular plug-like intrusions of porphyrite, dykes of lamprophyre and flow remnants of andesite (Jennings & Sutherland 1969). Sutherland & Corbett (1974) reported minimum ages ranging from 91 ± 1 Ma (K/Ar) to 103 ± 23 Ma (Rb/Sr), and McDougall & Green (in McClenaghan *et al.* 1982) obtained K/Ar ages of between 102.3 ± 2.6 and 101.3 ± 2.6 Ma from hornblende separates. Small lamprophyre dykes also crop out on Waterhouse Island (Baillie *et al.* 1978), north of Great Musselroe Bay, Cod Bay and George Rocks (Baillie 1984). Drilling at Cuckoo Creek, behind Great Musselroe Bay, encountered similar dykes, one of which yielded a K/Ar whole rock age of 98.7 ± 0.6 Ma (Baillie 1986).

Cretaceous syenites intrude both Late Carboniferous-Permian beds and Jurassic dolerite in the Cygnet-Kettering area of southern Tasmania (Ford 1983). Although mainly oversaturated, they include some silica-undersaturated dykes. K/Ar dating of mineral separates indicate an age of 100.5 ± 0.8 Ma (Evernden & Richards 1962, McDougall & Leggo 1965).

The younger (8 to > 58 Ma) Tasmanian Cainozoic basalts contain some relatively evolved nepheline mugearites and mafic nepheline benmoreites (Mg# 43-53; D. I. 53-58; Sutherland *et al.* 1989), but none approach the Tomahawk rock (Mg# 13.2, D. I. 82.8) in this respect.

The Tomahawk River dyke represents a new, albeit very minor, phase of igneous activity for Tasmania. However, some indirect evidence for other Late Cretaceous magmatism exists in the area. This comes from fission-track dating of distinctive pale yellow-brown zircon megacrysts (5 grains, 71.3 ± 5.9 Ma) found with other younger zircon megacryst suites (42–53 ± 2–4 Ma) in an alluvial sub-basaltic deposit at Grays Hill, near Branxholm (Australian Museum unpublished data, Geotrack International Report #169, June 1989). The older zircons lie within error of the Ar-Ar dating of the Tomahawk phonolite.

The 75–81 Ma age of the Tomahawk phonolite overlaps with the main period of the opening of the Tasman Sea, which spans Anomalies 34 to 24 (Gaina *et al.* 1998), corresponding to about 84 to 52 Ma (Cande & Kent 1995). Rifting and spreading commenced after 84 Ma, along the Tasman margin, off northeastern Tasmania (Duddy & Green 1992, Sutherland 1994, Royer & Rollet 1997, O'Sullivan *et al.* 2000, Norvick & Smith 2001).

More locally, Cretaceous rifting formed the Boobyalla Sub-basin, a southeasterly extension of the Bass Basin that extends on-shore near the mouth of the Ringarooma River, about 15 km ENE of the Tomahawk dyke (fig. 1; Moore *et al.* 1984, Luskin *et al.* 1989). Geophysical evidence suggests that, in this area, the sub-basin is 600–800 m thick and bounded by rotational normal faults (Leaman 1973, Leaman & Symonds 1975). Two drill holes penetrated a non-marine sequence of dolerite-boulder to granule-conglomerate and poorly sorted ferruginous sandstone of mainly Late Cretaceous biostratigraphic age. Angiosperm pollen at the base of the deepest hole (491 m) indicates an age probably no older than Turonian (89–91 Ma). Thus the Boobyalla Sub-basin appears to have been initiated in the Late Cretaceous, considerably later than the remainder of Bass Basin (Luskin *et al.* 1989) but prior to the opening of the Tasman Sea and the Tomahawk phonolitic magmatism.

Sharples & Klootwijk (1981) showed that Ordovician Gordon Group Limestone at Ida Bay, in far southern Tasmania, was completely remagnetised in the Late Cretaceous or Early Cainozoic, even though conodont colour indices indicate that the limestone had not been heated beyond 100°C. This was interpreted as further evidence for a prolonged episode of increased heat flow and widespread remagnetisation in southeastern Australia at this time, possibly related to the rifting prior to opening of Tasman Sea.

Thus, like many other alkaline rocks from continental settings, the Tomahawk River phonolite may be related to rifting and increased heat flow associated with continental break-up.

The Tomahawk alkaline activity does not correlate with any published Late Cretaceous intraplate basaltic activity in eastern Victoria, on the northern side of the intervening Gippsland Basin. Eastern Victorian basaltic intrusions and associated contact metamorphic activity are recorded between 85–95 Ma (McKenzie *et al.* 1984, Price *et al.* 1988, Duddy & Green 1992), but mark an earlier rift-related episode in relation to the initial Tasman spreading period and the Tomahawk magmatism. Phonolitic intrusions appear within some basalt provinces in eastern Victoria, but are not dated and may relate to the older Mesozoic phonolites at Gallows Hill, near Mansfield (~ 156 ± 20 Ma, recalculated from McDougall & Wellman 1976). Proven Late Cretaceous phonolitic magmatism, as at Tomahawk, is rare in eastern Australia. However, a comparative example forms the Mount Ramsay nepheline syenite, near Baralaba, central Queensland (72 Ma; table 11), which may relate to a central volcano plume trace (Sutherland *et al.* 1996).

ACKNOWLEDGEMENTS

The dating work was undertaken as a joint project between the Australian Museum Geodiversity Research Centre and the CSIRO Division of Petroleum Resources (Bentley, Perth, WA). The Ar-Ar data presented in this study were undertaken at the Western Australian Argon Isotope Facility, operated by a consortium of Curtin University and University of Western Australia.

Dr Jo-Anne Wartho (Curtin University) and Andrew Todd (CSIRO Petroleum) are thanked for assistance during K-Ar and ^{40}Ar-^{39}Ar analyses. R. S. Bottrill, G. R. Green, L. M. Hay, A. J. Hollick, S. Heawood, R. G. Richardson, J. Taheri and R. N. Woolley at Mineral Resources Tasmania are thanked for use of equipment, technical assistance and support. D. Steele and P. Robinson (University of Tasmania) assisted with electron microprobe and performed ICPMS analyses respectively. We also thank Prof. A. J. Crawford and an anonymous reviewer for their advice on the manuscript.

REFERENCES

ABLAY, G.J., CARROLL, M.R., PALMER, M.R., MARTI, J. & SPARKS, R.S.J., 1998: Basanite-phonolite lineages of the Teide-Pico Viejo Volcanic Complex, Canary Islands. *Journal of Petrology* 39: 905–936.

ANON., 1970: Catalogue of the minerals of Tasmania. *Geological Survey Record* 9, Tasmania Department of Mines.

BAILEY, D.K., 1974: Origin of alkaline magmas as a result of anatexis: (b) melting in the deep crust. *In* Sorensen, H. (Ed.): *The Alkaline Rocks.* John Wiley & Sons, London: 436–442.

BAILEY, D.K., 1976: Applications of experiments to alkaline rocks. *In* Bailey, D. K. & Macdonald, R. (Eds): *The Evolution of Crystalline Rocks.* Academic Press, London: 419–469.

BAILEY, D.K. & SCHAIRER, J.F., 1965: The system Na_2O-Al_2O_3-Fe_2O_3-SiO_2 at 1 atmosphere, and the petrogenesis of alkaline rocks. *Journal of Petrology* 7: 114–170.

BAILLIE, P.W., 1972: The structure of the granitic rocks of the Little Mt Horror area. *Tasmania Department of Mines Technical Reports* 15: 32–36.

BAILLIE, P.W., 1984: Geological Atlas 1:50,000 Series. Sheet 8516S (25). Eddystone. Tasmania Department of Mines, Hobart.

BAILLIE, P.W., 1986: Geological Survey Explanatory Report. Sheet 8516S (25). Eddystone. Tasmania Department of Mines, Hobart.

BAILLIE, P.W., TURNER, N.J. & COX, S.F., 1978: Geological Atlas 1:50,000 Series. Sheet 8416S (24). Boobyalla. Tasmania Department of Mines, Hobart.

BONHOMME, M.G., THUIZAT, R., PINAULT, Y., CLAUER, N., WENDLING, R. & WINKLER, R., 1975: *Méthode de datation potassium-argon. Appareillage et technique.* University of Strasbourg, 53pp.

BOYNTON, W.V., 1984: Geochemistry of the rare earth elements: meteorite studies. *In* Henderson, P. (Ed.): *Rare earth element geochemistry.* Elsevier, Amsterdam: 63–114.

CANDE, S.C. & KENT, D.V., 1995: Revised calibration of the geomagnetic polarity time scale for the Late Cretaceous and Cenozoic. *Journal of Geophysical Research* 100: 6093–6095.

DEER, W.A., HOWIE, R.A. & ZUSSMAN, J., 1997: *Rock-forming minerals. Volume 2B, second edition. Double-chain silicates.* The Geological Society, London, 764 pp.

DUDDY, I.R. & GREEN, P.F., 1992: Tectonic development of the Gippsland Basin and environs: identification of key episodes using apatite fission track analysis (AFTA). *In* Barton, C. (Ed.) *Energy, Economics and Environmemt: Gippsland Basin Symposium, 22-23 June 1992.* Australasian Institute of Mining and Metallurgy, Melbourne: 111–120.

EDWARDS, A.B., 1947: Alkali hybrid rocks of Port Cygnet, Tasmania. *Proceedings of the Royal Society of Victoria* 58: 81–115.

EVERARD, J.L., 2004: A ground magnetometer survey and compilation of field, petrographic and geochemical data from the Tomahawk River phonolite dyke, northeast Tasmania. *Tasmanian Geological Survey Record.*

EVERNDEN, J.F. & RICHARDS, J.R., 1962: Potassium-argon ages in eastern Australia. *Journal of the Geological Society of Australia* 9: 1–37.

EWART, A., CHAPPELL, B.W. & LE MAITRE, R.W., 1985: Aspects of the mineralogy and geochemistry of the intermediate-silicic Cainozoic volcanic rocks of eastern Australia; part 1: introduction and geochemistry. *Australian Journal of Earth Sciences* 32: 359–382.

FERGUSSON, A.K., 1978: The crystallization of pyroxenes and amphiboles in some igneous rocks and the presence of a pyroxene compositional gap. *Contributions to Mineralogy and Petrology* 67: 11–15.

FORD, R.J., 1983: The alkaline rocks of Port Cygnet, Tasmania. Unpublished Ph.D. thesis, University of Tasmania.

GAINA, C., MÜLLER, D.R., ROYER, J.-Y., STOCK, J., HARDEBECK, J. & SYMONDS, P., 1998: The tectonic history of the Tasman Sea: a puzzle with 13 pieces. *Journal of Geophysical Research* 103: 12413–21433.

GARCIA, M.O., FREY, F.A. & GROOMS, D.G., 1986: Petrology of volcanic rocks from Kaula Island, Hawaii. *Contributions to Mineralogy and Petrology* 94: 461–471.

GROVES, D.I., 1977: The geology, geochemistry and mineralization of the Blue Tier Batholith. *Geological Survey of Tasmania Bulletin* 53. Tasmania Department of Mines, Hobart.

HAMILTON, D.L. & MCKENZIE, W.S., 1965: Phase equilibria studies in the system $NaAlSiO_4$ (nepheline) - $KAlSiO_4$ (kalsilite) - SiO_2 (quartz). *Mineralogical Magazine* 34: 214–231.

HEINRICHS H. & HERRMANN, A.G., 1990: *Praktikum der Analytischen Geochemie.* Springer-Verlag, Berlin-Heidelberg, 669 pp.

HESS, J.C. & LIPPOLT, H.J., 1994: Compilation of K-Ar measurements on HD-B1 standard biotite 1994 status report. Phanerozoic Time Scale. G. S. Odin, Paris. *Bulletin of Liaison and Information, IUGS Subcommission of Geochronology* 12: 19–23.

JENNINGS, D.J. & SUTHERLAND, F.L., 1969: Geology of the Cape Portland area, with special reference to the Mesozoic(?) appinitic rocks. *Tasmania Department of Mines Technical Reports* 13: 45–81.

JOHNSON, R.W. & DUGGAN, M.B., 1989: Rock classification and analytical data bases. *In* Johnson, R.W. (Comp. & Ed.): *Intraplate Volcanism in Eastern Australia and New Zealand.* Cambridge University Press, Cambridge: 12–13.

KELLER, J., 1983: Potassic lavas in the orogenic volcanism of the Mediterranean area. *Journal of Volcanology and Geothermal Research* 18: 321–335.

KNUTSON, J. (Ed.), 1989: East Australian Volcanic Geology. *In* Johnson, R.W. (Comp. & Ed.): *Intraplate Volcanism in Eastern Australia and New Zealand.* Cambridge University Press, Cambridge: 89–115.

KYLE, P.R., 1981: Mineralogy and petrology of a basanite to phonolite sequence at Hut Point Peninsula, Antarctica, based on core from Dry Valley Drilling Project Drillholes 1, 2 and 3. *Journal of Petrology* 22: 451 - 500.

KYLE, P.R., MOORE, J.A. & THIRLWALL, M.F., 1992: Petrological evolution of anorthoclase phonolite lavas at Mt Erebus, Ross Island, Antarctica. *Journal of Petrology* 33: 849–875.

LEAKE, B.E. (Comp.), 1997: Nomenclature of amphiboles: Report of the Subcommittee on Amphiboles of the International Mineralogical Association, Commission on New Miner-

als and Mineral Names. *American Mineralogist* 82: 1019–1037.

LEAMAN, D.E., 1973: Summary of geophysical work, Gladstone area. *Tasmania Department of Mines Technical Reports* 16: 89–96.

LEAMAN, D.E. & SYMONDS, P.A., 1975: Gravity survey of northeastern Tasmania. *Geological Survey of Tasmania Paper 2.* Tasmania Department of Mines, Hobart.

LE BAS, M.J., LE MAITRE, R.W., STRECKEISEN, A. & ZANETTIN, B., 1986: A chemical classification of volcanic rocks based on the total alkali silica diagram. *Journal of Petrology* 27: 745–750.

LE MAITRE, R.W., 1976: The chemical variability of some common igneous rocks. *Journal of Petrology* 17: 589–637.

LE ROEX, A.P., CLIFF, R.A. & ADLER, B.J. I., 1990: Tristan da Cunha, South Atlantic: geochemistry and petrogenesis of a basanite-phonolite lava series. *Journal of Petrology* 31: 779–812.

LIPPARD, S.J., 1973: The petrology of phonolites from the Kenya Rift. *Lithos* 6: 217–234.

LUDWIG, K.R., 2001: Isoplot/Ex rev. 2.49, a Geochronological Toolkit for Microsoft Excel. *Berkeley Geochronology Centre Special Publication 1a.*

LUSKIN, A., HOBDAY, D.K. & BAILLIE, P.W., 1989: Boobyalla Sub-basin. *In* Burrett, C.F. & Martin, E.L. (Eds): *Geology and Mineral Resources of Tasmania.* Geological Society of Australia Inc., Special Publication 15: 356–358.

MCCLENAGHAN, M.P. & WILLIAMS, P.R., 1982: Distribution and characterisation of granitoid intrusions in the Blue Tier area. *Geological Survey Paper 4.* Tasmania Department of Mines, Hobart.

MCCLENAGHAN, M.P., TURNER, N.J., BAILLIE, P.W., BROWN, A.V., WILLIAMS, P.R. & MOORE, W.R., 1982: Geology of the Ringarooma- Boobyalla area. *Geological Survey of Tasmania Bulletin* 61. Tasmania Department of Mines, Hobart.

MCDOUGALL, I. & HARRISON, T.M., 1999: *Geochronology and Thermochronology by the $^{40}Ar/^{39}Ar$ method* (2nd Edition). Oxford University Press, New York, 269 pp.

MCDOUGALL, I. & LEGGO, P.J., 1965: Isotopic age determination on granitic rocks from Tasmania. *Journal of the Geological Society of Australia* 12: 295–332.

MCDOUGALL, I. & ROKSANDIC, Z., 1974: Total fusion $^{40}Ar/^{39}Ar$ ages using HIFAR reactor. *Journal of the Geological Society of Australia* 21: 81–89.

MCDOUGALL, I. & WELLMAN, P., 1976: Potassium-argon ages for some Australian Mesozoic igneous rocks. *Journal of the Geological Society of Australia* 23: 1–9.

MCKENZIE, D.A., NOTT, R.J. & BOLGER, P.F., 1984: Radiometric age determinations. *Geological Survey of Victoria Report* 74 (unpublished).

MACKENZIE, D.E., BLACK, L.P. & SUN, S.-S., 1988: Origin of alkali feldspar granites associated with the Poimena granite, northeastern Tasmania. *Geochimica et Cosmochimica Acta* 54: 2313–2322.

MARSH, J.S., 1975: Aenigmatite stability in silica- undersaturated rocks. *Contributions to Mineralogy and Petrology* 50: 135–144.

MOORE, W.R., BAILLIE, P.W., FORSYTH, S.M., HUDSPETH, J.W., RICHARDSON, R.G. & TURNER, N.J., 1984: Boobyalla Sub-basin: a Cretaceous onshore extension of the southern edge of the Bass Basin. *APEA Journal* 24: 110–117.

MORIMOTO, N., 1988: Nomenclature of pyroxenes. *American Mineralogist* 73: 1123–1133.

NICKEL, E.H. & MARK, E., 1965: Arfvedsonite and aegirine-augite from Seal Lake, Labrador. *Canadian Mineralogist* 8: 185–197.

NOLAN, J., 1966: Melting relations in the system $NaAlSi_3O_8$-$NaAlSiO_4$- $NaFeSi_2O_6$-$CaMgSi_2O_6$-H_2O and their bearing on the genesis of alkaline undersaturated rocks. *Quarterly Journal of the Geological Society* 112: 119–157.

NORVICK, M.S. & SMITH, M.A., 2001: Mapping the plate tectonic reconstruction of southern and southeastern Australia and implications for petroleum systems. *APPEA Journal* 41: 15–34.

O'SULLIVAN, P.B., MITCHELL, M.M., O'SULLIVAN, A.J., KOHN, B.P. & GLEADOW, A.J.W., 2000: Thermotectonic history of the Bassian Rise, Australia: implications for the breakup of eastern Gondwana along Australia's southeastern margins. *Earth and Planetary Science Letters* 182: 31–47.

PRICE, R.C., JOHNSON, R.W., GRAY, C.M. & FREY, F.A., 1985: Geochemistry of phonolites and trachytes from the summit region of Mt Kenya. *Contributions to Mineralogy and Petrology* 89: 394–409.

PRICE, R.C., GRAY, C.M., NICHOLLS, I.A. & DAY, A., 1988: Cainozoic volcanic rocks. *In* Douglas, J.G. & Ferguson, J.A. (Eds): *Geology of Victoria.* Geological Society of Australia, Victorian Division. Melbourne: 439–451.

QUILTY, P.G. & WHELLER, G.E., 2000: Heard Island and the McDonald Islands: a window into the Kerguelen plateau. *Papers and Proceedings of the Royal Society of Tasmania* 122(2): 1–12.

ROYER, J-Y. & ROLLET, N., 1997: Plate-tectonic setting of the Tasmanian region. *Australian Journal of Earth Sciences* 44: 543–560.

SCHAIRER, J.F., 1950: The alkali feldspar join in the system $NaAlSiO_4$-$KAlSiO_4$ -SiO_2. *Journal of Geology* 58: 512–517.

SCHAIRER, J.F. & BOWEN, N.L., 1956: The system Na_2O-Al_2O_3-SiO_2. *American Journal of Science* 254: 129–195.

SHARPLES, C. & KLOOTWIJK, C.T., 1981: Palaeomagnetic results from the Gordon Subgroup of Tasmania: further evidence for a late Cretaceous magnetic overprint in southeastern Australia. *Papers and Proceedings of the Royal Society of Tasmania* 115: 85–91.

SIMKIN, T. & SMITH, J.V., 1970: Minor element distribution in olivine. *Journal of Geology* 78: 304–325.

SISSON, T.W., 1994: Hornblende-melt trace-element partitioning measured by ion microprobe. *Chemical Geology* 117: 331–344.

SORENSEN, H. (Ed.), 1974: *The Alkaline Rocks.* John Wiley & Sons, London. 622 pp.

STEIGER, R.H. & JÄGER, E., 1977: Subcommission on Geochronology: convention on the use of decay constants in geo- and cosmochronology. *Earth and Planetary Science Letters* 36: 359–362.

STEPHENSON, P.J., GRIFFIN, T.J. & SUTHERLAND, F.L., 1980: Cainozoic volcanism in northeastern Australia. *In* Henderson, R. A. & Stephenson, P.J. (Eds) *The Geology and Geophysics of Northeastern Australia.* Geological Society of Australia, Queensland Division: 349–374.

SUN, S.-S. & MCDONOUGH, W.F., 1989: Chemical and isotopic systematics of oceanic basalts: implications for mantle composition and processes. *In* Saunders, A. D. & Norry, M. J. (Eds) *Magmatism in the Ocean Basins.* Geological Society of London Special Publication 42: 313–346.

SUTHERLAND, F.L., 1976: Cainozoic volcanic rocks. *In* Leaman, D.E. Geological Survey Explanatory Report. Sheet 82 (8312S). Hobart. Tasmania Department of Mines, Hobart: 35–36.

SUTHERLAND, F.L., 1994: Tasman Sea evolution and hotspot trails. *In* Van der Lingen, G.J., Swanson, K.M. & Muir, R.J. (Eds): *Evolution of the Tasman Sea Basin.* A.A. Balkema, Rotterdam: 35–51.

SUTHERLAND, F.L. & CORBETT, E.B., 1974: The extent of Upper Mesozoic igneous activity in relation to lamprophyric intrusions in Tasmania. *Papers and Proceedings of the Royal Society of Tasmania* 107: 175–190.

SUTHERLAND, F.L., EWART, A., RAYNOR, L.R., HOLLIS, J.D. & MCDONOUGH, W.D., 1989: Tertiary basaltic magmas and the Tasmanian lithosphere. *In* Burrett, C.F. & Martin, E.L. (Eds): *Geology and Mineral Resources of Tasmania.* Geological Society of Australia Special Publication 15: 386–398.

SUTHERLAND, F.L., ROBERTSON, A.D., BARRON, B.J. & POGSON, R.E., 1996: The Rockhampton plume and its late Mesozoic trace? *In* Mesozoic Geology of the Eastern Australian Plate, Mesozoic 96 Conference, 23 - 26 September, Brisbane. *Geological Society of Australia Extended Abstracts* 43: 519–527.

TAHERI, J. & BOTTRILL, R., 1999: Porphyry and sedimentary-hosted gold deposits near Cygnet: new styles of gold mineralisation in Tasmania. *Tasmanian Geological Survey Record* 1999/01.

THOMPSON, G.M., SMITH, I.E.M. & MALPAS, J.G., 2001: Origin of oceanic phonolites by crystal fractionation and the problem of the Daly gap: an example from Rarotonga. *Contributions to Mineralogy and Petrology* 142: 336–346.

WEAVER, B.L., 1990: Geochemistry of highly under-saturated oceanic island basalt suites from the South Atlantic Ocean: Fernando de Noronha and Trinidade islands. *Contributions to Mineralogy and Petrology* 105: 502–515.

WILSON, M., DOWNES, H. & CEBRIA, J., 1995: Contrasting fractionation trends in coexisting continental alkaline magma series; Cantal, Massif Central, France. *Journal of Petrology* 36: 1723–1753.

WONES, D.R. & EUGSTER, H.P., 1965: Stability of biotite: experiment, theory and application. *American Mineralogist* 50: 1228–1272.

WÖRNER, G. & SCHMINCKE, H.-U., 1984a: Mineralogical and chemical zonation of the Laacher See tephra sequence (East Eifel, W. Germany). *Journal of Petrology* 25: 805–835.

WÖRNER, G. & SCHMINCKE, H.-U., 1984b: Petrogenesis of the zoned Laacher See tephra. *Journal of Petrology* 25: 836 –851.

YOUNG, G.C. & LAURIE, J.R., (Eds), 1996: *An Australian Phanerozoic Timescale.* Oxford University Press, Melbourne, 279 pp.

YU Z., ROBINSON P. & MCGOLDRICK P., 2001: An evaluation of methods for the chemical decomposition of geological materials for trace element determination using ICP-MS. *Geostandards Newsletter, the Journal of Geostandards and Geoanalysis* 25: 199–217.

(accepted 2 February 2004)